2016-01-01

Characterization In 2d Sulfides And Graphene Composites For Sensing Applications

Alberto Delgado
University of Texas at El Paso, adelgado22@miners.utep.edu

CHARACTERIZATION IN 2D SULFIDES AND GRAPHENE COMPOSITES FOR SENSING APPLICATIONS

ALBERTO DELGADO

Master's Program in Metallurgical and Materials Engineering

APPROVED:

Anupama B. Kaul, Ph.D., Chair

Shailendra K. Varma, Ph.D.

Stephen W. Stafford, Ph.D.

Stella Quinones, Ph.D.

Charles Ambler, Ph.D.
Interim Dean of the Graduate School

DEDICATION

Through my thesis work, self-efforts such as taking initiative, developing new ideas for experiments, and perseverance were required. However, the guidance of those who are very close to my heart is the most important part and key for success, which provides motivation and support to continue working and to excel on every task assigned.

This humble effort of thesis work I dedicate to my family, especially to my loving parents, Ivione and Armando, whose affection, love, encouragement, and prayers make me able to complete one more step in my career life, along with the fortification, love, and affection of my brothers: Armando, Angel Gabriel, and Alex Delgado. Correspondingly, this thesis work is similarly dedicated to my friends, particularly to my beloved girlfriend, Abigail Tellez, whose stimulation, happiness, and assistance resulted in the liveliness to surpass any experiment, pressure, stress, and wakefulness.

Among these special people I dedicate my work to the professors and co-workers, whose teachings and partnership offered me inspiration and creativity to develop a new perspective of the study performed in this thesis work.

"IN ALL CIRCUMSTANCES GIVE THANKS, FOR THIS IS THE WILL OF GOD FOR YOU IN CHRIST JESUS" (1 THESSALONIANS 5:18)

CHARACTERIZATION IN 2D SULFIDES AND GRAPHENE COMPOSITES FOR SENSING APPLICATIONS

by

ALBERTO DELGADO, B.S. M.E., B.S. M.M.E.

THESIS

Presented to the Faculty of the Graduate School of

The University of Texas at El Paso

in Partial Fulfillment

of the Requirements

for the Degree of

MASTER OF SCIENCE

Department of Metallurgical, Materials and Biomedical Engineering

THE UNIVERSITY OF TEXAS AT EL PASO

May 2016

ACKNOWLEDGEMENTS

Support is acknowledged from the University of Texas System Faculty Science and Technology Acquisition and Retention (STARS) award (EC284802) for the acquisition of equipment in the establishment of the Nanomaterials and Devices Lab (NDL) at the University of Texas, El Paso (UTEP). I also thank the Army Research Office (Grant number 226020381A) that enabled us to pursue this work.

Within these acknowledgements, I also thank Los Alamos National Laboratory at New Mexico for providing Raman measurements of the studied materials, Armando Delgado Ph. D. candidate student for offering his help to deliver particle size distribution measurements, and finally Angel Lerma from the Machine Shop at UTEP for assisting me in the machining of molds and fixtures for opto-electro-mechanical measurements of composite materials.

ABSTRACT

In this work, we have evaluated 2D layered material composites for opto-electro-mechanical sensing applications. In particular, we have focused on TMDCs and graphite and studied the effects of chemical liquid exfoliation on the structural characteristics of the 2D layered materials, through particle size, x-ray diffraction, Raman and surface area analysis. An approach was developed to combine the solution-processed dispersion with organic and inorganic matrix materials for forming the composites. From Raman Spectroscopy of the ultra-sonicated samples, the $I_{2D}/I_G>2$ for graphite, and for MoS_2 the difference between the A_{1g} and E_{2g} peak was 22.85cm^{-1}, consistent with few layer 2D MoS_2. In terms x-ray diffraction measurements of possible exfoliated materials, TMDCs and graphite, provided similar behavior when stress was induced while ultra-sonication took place, whereas aluminum powder particles, which were also analyzed for comparative purposes, tended to not follow this behavior. Once the characterization was completed, the treated samples were introduced into two dissimilar polymer matrix materials, an elastomer and an acrylic material. The graphite composite samples produced electrical signals on both of the matrices, i.e. the elastomer was combined with the graphite powder and yielded a novel composite that was tested for its opto-electro-mechanical response. The graphite elastomer based composite produced sensitivities of 0.90 V μA-1 at 7 V, 0.65 V μA-1 at 5 V and 0.39 V μA-1 at 3 V. On the other hand, the graphite-acrylic composites were tested in bending mode where the optical and electronic characterization data was gathered as a function of strain and loading density. Tunneling based mechanisms and percolation theory were used to explain the behavior of the composites in terms of the strain response as a function of the loading density. This work forms a solid foundation from which to pursue more advanced studies on the opto-electro-mechanical response of 2D layered material based composites for a wide range of applications, such as strain sensors used in health monitoring and non-destructive evaluation of materials.

TABLE OF CONTENTS

LIST OF FIGURES

CHAPTER 1: INTRODUCTION

1.1 Motivation

Promising materials in the two-dimensional (2D) layered materials family such as graphite, MoS_2 and WS_2 have already been utilized in a wide range of applications. For such materials to have promise in applications, a facile approach for producing large quantities of these materials is necessary. Specially, one of the actively pursued approaches to produce these materials has been through chemical exfoliation using ultra-sonication in liquid organic solutions, such as N-Methyl-Pyrrolidone (NMP). When exfoliating these materials into a 2D layer structure, they can provide excellent optical and electrical properties for semiconducting applications. In other words, these applications correspond to sensing devices in mechanical and biomedical environments by producing optical and electrical signals capable to be detected.

Even though the studies made in chemical liquid exfoliation in NMP are numerous, there are studies that can be done to determine the mechanisms and performance of this technique (Hu et al. 2013). Among the studies that can be performed to develop better understanding in 2D layered material processes, there are characterization techniques that have not been contemplated, which could produce potential growth in development and performance. Chemical liquid exfoliation is a practical way to fragmentize bulk materials such as TMDs and graphite, more over it is also a simplistic and interesting approach to produce 2-D layered materials (Cunningham et al. 2012).

The devices that are mostly produced by these exfoliated materials consist of composites in thin films or heterogeneous structures; however, is also foreseen that 2D layered material properties can also be implemented in 3D composite devices. Therefore, understanding and executing new techniques to characterize 2D materials would maximize the introduction of 2D layered materials into composite applications.

1.2 Objectives

Two dimensional (2D) layered materials and non-layered materials are implemented in this study by chemical liquid exfoliation method in NMP solvent. Once these materials are ultra-sonicated, interactions are taking place within particles in the dispersions. The goal of this experimental work described in this thesis is to investigate materials particles during solution processing and composite formulation, which include the following studies:

- To determine ultra-sonication effects when exposing MoS_2, WS_2, graphite and aluminum into chemical liquid exfoliation by ultra-sonication bath system
- To implement the treated ultra-sonicated materials in polymer matrix for the creation of composites to investigate their optical and electrical properties as a function of strain

CHAPTER 2: BACKGROUND

As nanotechnology is exponentially increasing, new applications and research are evolving. As the new generation of applications is emerging in the research area, as well in the market, also new materials and different processes are in need to be explored. Right now, in the 21st century, there are high demands in the biomedical applications. Researchers are correctly thinking about the improvement of life quality; therefore, in order to come up with better performance of human body, it is necessary to understand body movement at its full extent. When talking about human body movement, interactions of forces and stresses come into place, in which the human body is subjected to when experiencing displacement throughout the body. So then new technology, especially nanotechnology, is trying to achieve better quality on devices that perform personal health monitoring, rehabilitation monitoring, and sports performance monitoring (C. X. Liu and Choi 2009; Giorgino et al. 2009; Lorussi et al. 2005; C.-X. Liu and Choi 2009; Rautaray and Agrawal 2011). There also are many other applications in which nanotechnology can be implemented, such as in apparatus where life of a material needs to be monitored; for example, looking into creep, fatigue, sensing, catalysis, and energy storage applications (Rautaray and Agrawal 2011; Rosenberger et al. 2012). All these biomedical and mechanical applications make the researches take an especial look and consider how these types of sensing devices can take place with distinctive optical, mechanical, and electronic properties, which is the leading question that take us to the investigation of what type of materials are ideal to perform in this category of materials are needed to enhance this new applications (Rogers, Someya, and Huang 2010).

These material's systems need to have exceptional mechanical, optical, and electrical properties to perform such measurements. Nanotechnology is looking for flexible, stretchable, and sensitive materials that can yield to such analyses (Rogers, Someya, and Huang 2010; Yao and Zhu 2014). Strain

sensor materials are the key for the success of non-expensive, high performance, and life-long monitoring systems (Pantelopoulos and Bourbakis 2010; Kaltenbrunner et al. 2013). Strain sensors consist of 3 main steps in order to perform its functionality, which are motion of the material, electrical and optical signals, and measurement. The external forces acting on the material will generate a motion within the structure of the material by the introduction of new dislocations, cracks, strain, or geometrical changes. The change in structure, if the material is sensitive enough, produces differences in optical and electrical properties. Having optimal electrical and optical properties for such application, when motion takes place these properties are affected, producing electrical and optical signals (Kaltenbrunner et al. 2013; Yamada et al. 2011; Amjadi et al. 2014; Hempel et al. 2012). Electrical and optical signals are then converted to produce a strain measurement of deformed materials; this measurement can be related to compression, tension, creep rupture, or fatigue damage. The response of material devices is a consequence of the mechanical deformations that make the electrical resistance change; there could be also changes in capacitance when the device is subjected to external stains. Finally, these signals are emitted as part of the sensor functionality to recognize changes in the material device so that those can be transported to monitoring systems.

After reviewing the main concepts of the strain sensors and the motivation that has proposed by the development of new and better stain sensor materials, it is time to focus on the materials that are being used and the way to process good quality materials. Therefore, it is critical to understand the behavior of the materials subjected to these kinds of applications. Composites offer a facile means to tailor the properties of hybrid, dissimilar material systems for applications ranging from optoelectronics to strain sensors. As one of the main studies in nowadays, graphene has become a material with high importance in the development of new devices, not only in strain sensors but through all the nanotechnology field (Geim 2009; Novoselov et al. 2012). Graphene is a unique and promising material for the nanocomposite strain sensors (Khan et al. 2010). Graphene consists of a structure, which is

hexagonally bonded carbon atoms in a thin atomically layer. This structure is capable a reaching exceptional electrical properties. Due to the transparent conducting electrons, graphene can tolerate enormous amounts of deformation. These mechanical and electrical properties make of graphene a perfect candidate for strain sensor materials (Hill, Vijayaragahvan, and Novoselov 2011).

Its been demonstrated through experimental results what graphene is capable of doing; however, research has still been done to graphene properties to excel its properties and performance in different fields (Geim and Novoselov 2007; Katsnelson 2007; Castro Neto et al. 2009). That is why also theoretical approaches have been done in order to understand more the nature of this material. With these interesting properties in the polycrystalline graphene, theoretical studies have shown that grain boundaries in graphene, which is a 1-dimentional defect in the graphene structure, have fascinating electronic, magnetic, chemical, mechanical, and thermal properties (Albrecht et al. 1988; Clemmer and Beebe 1991; Lahiri et al. 2010; Červenka and Flipse 2009; Peres, Guinea, and Castro Neto 2006; Yazyev and Louie 2010b; Mesaros et al. 2010; Malola, Häkkinen, and Koskinen 2010; Y. Liu and Yakobson 2010; Yazyev and Louie 2010a; Grantab, Shenoy, and Ruoff 2010; Bagri et al. 2011). These grain boundary defects do not affect the periodicity of the structure, and still well enough to lead the momentum conservation, which leads to the high charge transmission across the grain boundary (Yazyev and Louie 2010b). Now, as the crystallographic orientations change, the grain boundary can be either transparent or perfectly reflective for charged carrier over large energy range (Huang et al. 2010). With this and knowing that graphene does not have a band gap, graphene grain boundaries can be properly designed in order to modulate the transport gap, without an introduction of a band gap (Pereira and Castro Neto 2009).

Graphene not only has outstanding properties, it also has some practical preparation and easy manufacture (Paton et al. 2014). In the case of rubber bands with dispersed graphene the preparation was subjected to two main steps: 1) liquid exfoliation of graphene and then 2) the infusion of graphene into

the rubber band. In order to do the liquid exfoliation of graphene as discussed by Boland et al, the graphene is dispersed in the solvent N-Methyl-Pyrrolidone (NMP) using exfoliation techniques (Hernandez et al. 2008; Jonathan N. Coleman 2013).

Furthermore, many studies in graphene's structure and properties gave birth to a new set of studies of many other different compound materials; it is the case for the Transition Metal Dichalcogenides (TMDCs). These novel materials consist of well-bonded hexagonal transition metal atoms in between two layers of chalcogen atoms, which can be S, Se, or Te. This general structure covalently bonded is then stack into different layers by van der Waals forces. The TMDCs are compounds that can be classified as metallic, semi-metallic, and semiconductor due to the oxidation state and coordination number. In this study the focus on the semiconductors in MoS_2 and WS_2 will be investigated. As the number of layers of these bulk materials are reduced, electronic properties become more interesting providing special features that make them be considered for composite and sensing applications. These characteristics in TMDCs make also these materials to be included in exfoliation studies to achieve monolayer materials (Jariwala et al. 2014).

Considering MoS_2, as mentioned previously, it is a semiconducting material that is being considered for its promising optical and electrical properties as the number of layers decreases. Its structure, as its stoichiometry shows, corresponds to two atomic planes of sulfur with an in between atomic plane of molybdenum. As a bulk material, MoS_2 provides an indirect band gap; however, as the number of layers decreases it becomes a direct band gap. This monolayer with unique structures has a thickness of 0.62 nm, bigger than graphene, which has 0.34 nm as a monolayer, the only difference is that graphene do not have a band gap to offer as this semiconductor, MoS_2 (Tao et al. 2014)**.**

MoS_2 facilitates development for optoelectronic applications to deliver ultrasensitive sensors. (Jawaid et al. 2015) On the other hand, of semiconducting TMDCs, there exists WS_2 that is been studied but still not many experimental data has been recorded. WS_2 seems to have better chemical

stabilities than MoS_2, with also unique electronic properties suitable for optical components, I-C chips, catalysts and devices for and biological systems (Carey et al. 2015)**.**

In a monolayer form WS_2 has a band gap of at least 2.0 eV, whereas in MoS_2 the band gap energy corresponds to 1.81 eV (C.-X. Liu and Choi 2009; J. N. Coleman et al. 2011). WS_2 is sandwiched tungsten atomic plane by two sulfur atomic planes compared to molybdenum in sulfur; the atomic mass of tungsten is much higher than molybdenum atom. Therefore, due to its larger mass the valance band of WS_2 is ~425meV, where for MoS_2 is ~ 150 meV (Ovchinnikov et al. 2014). Due to this same fact of atomic mass, it usually corresponds to a high interatomic bonding as the mass increases; consequently, WS_2 provides higher interatomic bonding than MoS_2.

Several methods are been proposed to disrupt van der Waals bonds in the materials. Ali Jawaid et al provided with three different methods to produced exfoliation**,** in which three different medias were investigated. The first one was developed and produced great number of developments once graphene was exfoliated from graphite A. K. Geim and K. S. Novoselov by mechanical exfoliation (Jawaid et al. 2015; Geim and Novoselov 2007). Mechanical exfoliation constitutes in breaking van der Waals forces by utilizing adhesive tape or by grinding media (Jawaid et al. 2015). Even though this method is reliable, the production of monolayer or 2D layer materials cannot be implemented in a massive manner due to the constraints that adhesive tapes or grinding can provide only minute samples for laboratory use. Additionally, using grinding media to mechanically exfoliate materials such as graphite or TMDCs can become a problem when grinding media starts peeling off because purity of exfoliated materials can increase or can be difficult to filter few or monolayer flakes.

The second method discussed by Ali Jawaid et al consisted of unsetting the van der Waals, in which the ions interfere in the 2D materials as interlayer inclusions that modify crystallographic structure. Then, when subjected to vibration or particle movements, the layers peel off; however, further processes are needed to disassociate the intercalated ions from the layers. This method requires longer

time production, due to the several processes and inert environment needed (Jawaid et al. 2015). Therefore, this costly method provides more constraints in the development of 2D materials.

The third method entails chemical liquid exfoliation, in which bulk materials is exposed in a solvent solution. The dispersed material in the solvent solution is then subjected to ultra sonication, via bath sonication or probe sonication. Many organic solvents are being used to facilitate well exfoliation of bulky materials into few or monolayer structured material (Jawaid et al. 2015). While ultra sonication is taking place many factors affect are affecting the exfoliation technique, such as, type of organic solvent used, temperature, form of bulk material (powder or pellets) and ultra sonication power. Surface tension also plays a role in this method, in which there exists higher yield when surface tension of the liquid in the solvent is closer to the value of the surface energy of the solid. The higher yield produces higher interaction, and as ultra sonication is taking place the external forces to mechanical movement overcome internal forces such as van der Waals, as a result, few or monolayers of the dispersed materials are generated. In the last few years this method has become very well developed, especially with the assortment of organic solvents that can be utilized to produce exfoliation on materials with 2D layer capability. Among the implemented organic solvents the most common are Cyclohexanone, N-methyl-pyrrolidinone (NMP), Dimethylformamide (DMF), Isopropanol (IPA) and Dimethylacetamide (DMA). However, several studies have determined that NMP constitutes in one of the most promising and recommended organic solvents, due to its high yield in the presence of oxygen and water (Carey et al. 2015; J. N. Coleman et al. 2011). Materials such as graphite, MoS_2 and WS_2 have already being exposed to chemical liquid exfoliation in NMP and generating atomic layers; however, there are still many studies to determine the mechanisms and performance of this technique (Hu et al. 2013)**.** It is known that chemical liquid exfoliation is a practical way to fragmentize and shear bulk materials such as TMDs and graphite; moreover, it is also a simplistic and interesting approach to produce 2-D layered materials (Cunningham et al. 2012). Therefore, 2D layer materials and non-layer materials were

implemented in this study to compare and to understand the effects of chemical liquid exfoliation method in NMP solution.

CHAPTER 3: EXPERIMENTAL PROCEDURES

Powder materials subjected to ultra-sonication process in (NMP) solution, MoS_2, WS_2, Graphite, and Aluminum powder, were compared by utilizing characterization techniques. Each material was investigated at different times of ultra-sonication, running from 0 min to 18 hours using Branson 4500H ultra sonication system. In order to carry out these comparisons, the powder:NMP solution was dispersed at a concentration of 37.5 mg of powder per mL of NMP on a 50 mL beaker.

By employing different sonication times, changes in particles were observed in the dispersed solution. Therefore, the characterization performed in this study consisted in understanding the particle and structural behavior upon ultra sonication of powder particles. By characterizing the changes on the tested powder materials effects on ultra sonication were identified. The instrumentation for this analysis consisted of Microtrac and Scanning Electron Microscopy. During SEM powder evaluation morphology and particles size were investigated. SEM micrographs have been reported on the materials considered for this study. However, the uniqueness of this investigation also focuses on the particle size distribution measurement by utilizing Microtrac S3500 (Bluewave model) with a capability of performing wet measurements and provides particle dimensions ranging from 0.02 to 2800 μm.

The dispersed powder to be measured is carried by IPA through a light scattering technique system in which 3 lasers (2 blue and one red laser) are emitted to the powder particles. The red laser scatters the light from 0 to 60-degrees to acquire the large particle sizes whereas the blue lasers with smaller wavelength detect particles under the submicron and nanoparticles in the dispersed powder. Both blue lasers are aligned together, but facing opposite directions, then with this lower wavelength and positions provides repeatable, accurate, and reliable data. The distribution effects upon ultra sonication provide a new study and path for developing liquid chemical exfoliation by ultra sonication.

Along with the particle size distribution and the morphology evaluation, another set of investigation was performed to revise special characteristics at the atomistic level. This examination complemented the experiment by providing atomistic effects upon ultra sonication by the use of XRD, which was employed to see any shift or peak widening of the different ultra-sonication times. By modifying physical characteristics in powder is not sufficient for the creation of hybrid composites. Therefore, Raman spectroscopy was introduced to see how ultra sonication times facilitated the chemical exfoliation of 2D materials.

In order to provide and analyze reliable data, MoS_2, WS_2, graphite, and aluminum powders were divided into 5 different sample sets, in which each set of material powder was exposed to a different ultra-sonication time. The first sample of each powder material was a bulk, plain, and untreated model, which served as the control sample; this sample was not exposed to ultra-sonication treatment. The subsequent four samples corresponded to the following ultra-sonication treatment times: 30 minutes, 6 hours, 12 hours, and 18 hours. These ultra-sonicated powders were transferred to IPA solution for measuring particle size and deposition onto Si and SiO_2 wafers in order to analyze via SEM and Raman spectroscopy, respectively. Then, for XRD analysis the IPA with the dispersed powder was evaporated at room temperature and the powder alone was evaluated by x-ray diffraction mechanism.

Once structural characteristics were analyzed on each of the powders, hybrid composites were incorporated to analyzed possible applications for optical, mechanical, and electrical devices on elastomers and acrylic materials. After characterization of powder particles of 4 different materials such as MoS_2, WS_2, graphite, and aluminum powders exposed to the ultra sonication in NMP solution, the powders were integrated into two different hybrid composites. Figure 3.1 shows the first composite, in which the ultra-sonicated powder is introduced into a elastomer matrix, in this case a rubber band.

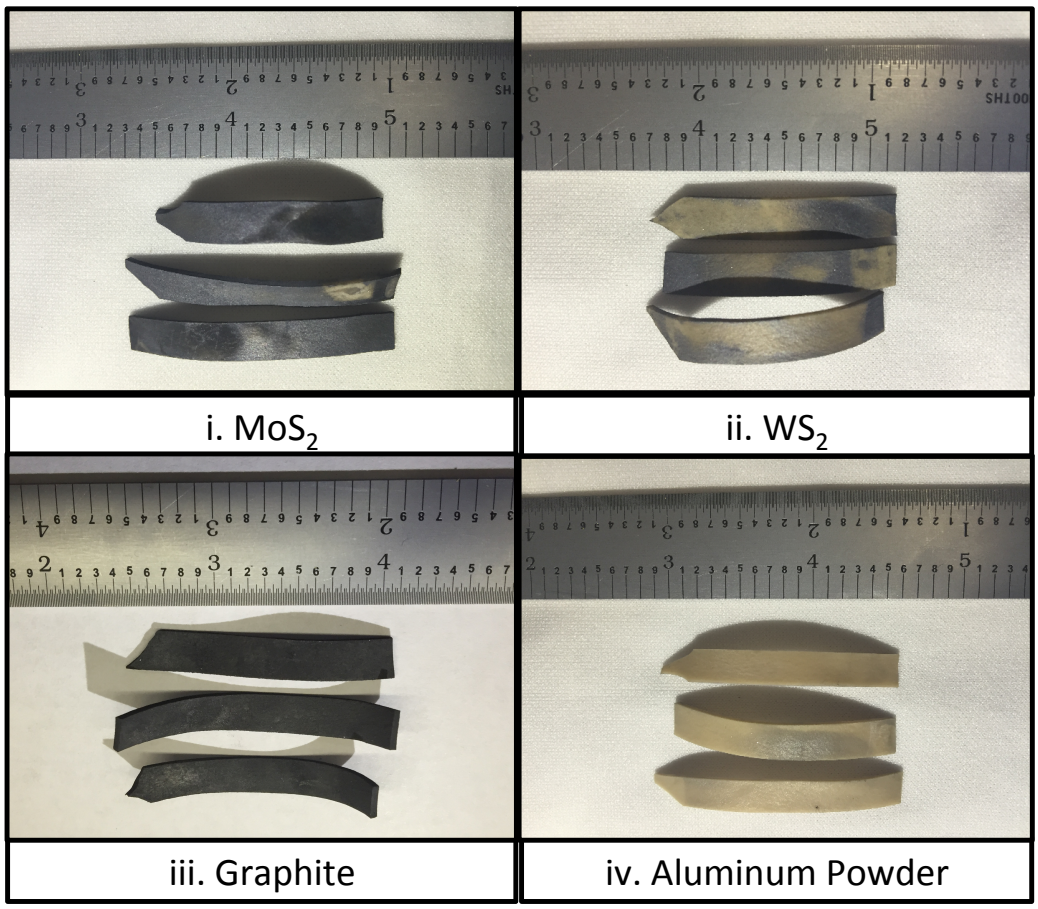

Figure 3.1 18-hour ultra-sonication powder was introduced into treated rubber bands with Toluene and NMP solutions.

Two samples of graphite/graphene were developed at different graphite/graphene dispersed concentrations, 37.5 mg mL-1 and 75 mg mL-1. For rubber band composites, the experimental method was followed by Boland et al experiment, where rubber bands were soaked in Toluene solution for 3.5 hours to expand the matrix by swelling mechanisms (Boland et al. 2014). After swelling, rubber bands were introduced to the 18 hour ultra-sonicated powders dispersed in NMP-water for a period of 48 hours; during this time the particles transferred to the elastomer matrix. As mentioned by Boland et al, water was added to make the particles energetically favorable to move from the solution to the elastomer pores (Boland et al. 2014). Finally, the rubber band was placed into the oven for 72 hours at 60 degrees to let it dry; this way water and NMP were removed. This composite was then exposed to electrical measurements as a function of mechanical movement. A standard local-machined device, shown in

figure 3.2, carried out this mechanical movement in which the elastomer was exposed to tensile movement at different strain levels.

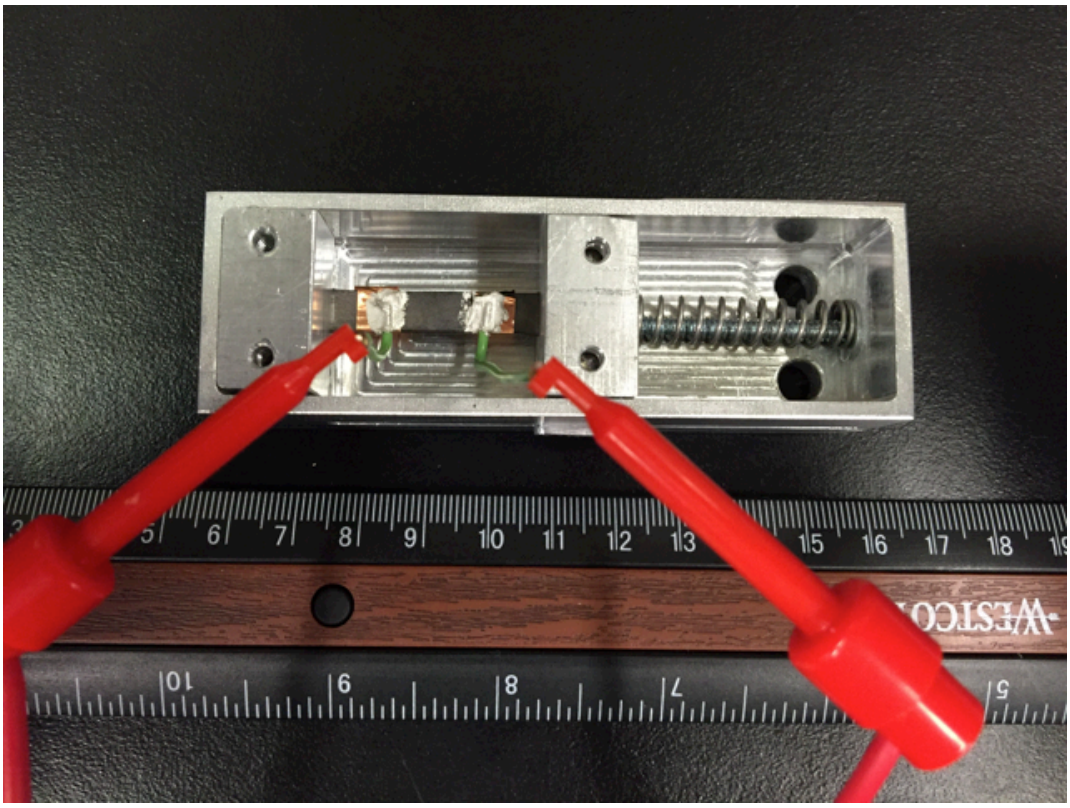

Figure 3.2 Local-standardize device to subject rubber bands to tensile force.

While developing the rubber bands, the dispersion of the treated materials powder in the composite was not uniform, except for the case of the graphite, which was well distributed and had interesting electrical measurements; this will be discussed furthermore in this paper. As far as the rest of the elastomer composites, there was a poor concentration and dispersion among the rubber band. Due to this, no electrical data was produced, but new investigation was open to see how this experimental method can be implemented in which good electrical data can be produced.

The second composite in Figure 3.3 corresponds to an acrylic solution, which once the dispersion of the powder is present addition of hardener is needed to solidify the composite. Acrylic composites were developed by the incorporation of 18-hour ultra-sonicated powder at different concentrations (250, 300, 350, and 400mg mL^{-1}). Graphite/graphene powder was dispersed into 3 mL of acrylic solution.

When creating the ultra-sonicated powder:acrylic mixture, it was then dropped into local manufactured molds. These molds were machined using US standard tools for a sample size dimensions outcome of 2.5 in (6.35 cm) in length, 0.5 in (1.27 cm) in width, and 0.05 in (0.127 cm) in depth. The poured ultra-sonicated powder:acrylic mixtures were exposed to the incorporation of 2 drops of hardener for solidification purposes and overnight drying at room temperature. With successful completion of hybrid composites in acrylic matrix, as shown in Figure 3.3, electrical measurements were obtained by creating contacts with silver ink and then subjecting the sample onto the probe station at different deformation stages, the distance between probes was fixed to 1 cm.

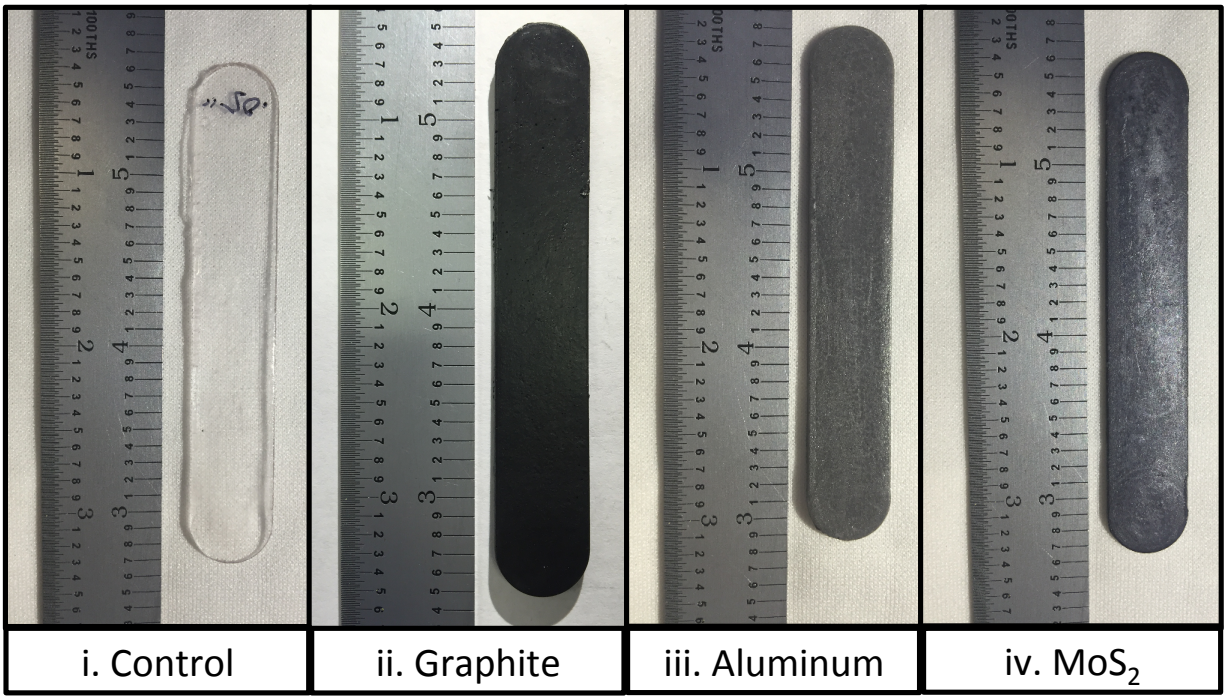

Figure 3.3 Hybrid composites with acrylic matrix and 18-hour ultra-sonicated treated graphite, aluminum and MoS_2 powders. Control sample corresponds to the acrylic matrix sample without any introduction of treated material powders.

Besides I-V measurements performed, optical measurements were analyzed with respect to mechanical bending. Therefore, in order to carry on analyses as a function of elastic deformation, five local 3D printed fixtures with different radius of curvature were designed. As seen in Figure 3.4, the measurements for electrical and optical properties of these particular hybrid composites were produced

by the local-fabricated fixtures with different radius of curvature, in which the powder:acrylic composites samples were placed on top of the fixture and fixed at the endpoints to reproduce reliable data.

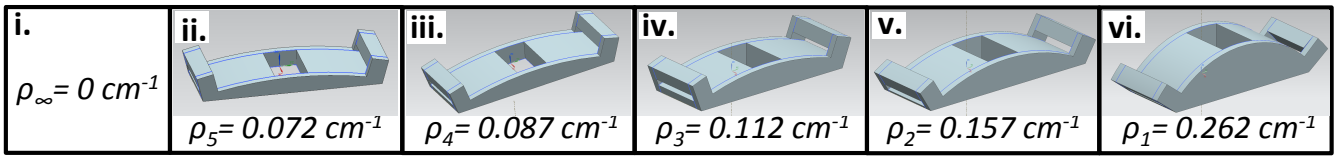

Figure 3.4 Design of local-standardized fixtures at various radius of curvature for bending mechanisms in optical and electrical measurements.

However, the material powders reacted in with unique characteristics. In the case of graphite/graphene:acrylic mixture generated the expected composite sample, a flexible and solid materials. Graphite/graphite-acrylic composite also caused successive and reproducible measurements in the optical and electrical signals. Aluminum composites reacted in a similar way, well-meaning samples were developed with higher flexibility than graphite. However, electrical properties were expected to be acceptable, which in this case did not happen. Even though aluminum is a conductive material, in this circumstance the composite material did not show electrical measurements.

Several suggestions can be developed at this point which can lead to a start of a new study. Surface tension of the following acrylic at the aluminum powder surface can be high enough to isolate each powder agglomeration between one another. Another suggestion can be developed by the reaction of the acrylic and aluminum causing a nonconductive secondary phase at the surface of the aluminum particles. In the case of TMDCs, unexpected results were observed during the final steps of the acrylic integration. MoS_2 did not complete solidified after the drying process, but effective removal from the mold was accomplished. For WS_2, no solidification occurred and a highly viscous material was produced. Therefore, no electrical or optical measurements were produced after the intent of creating TMDCs hybrid composites. This unique observation brings to the study of what is causing the viscous materials, but also novel characteristics can be achieved by incorporating this TMDCs-acrylic reaction

in the graphite/graphene:acrylic composites to enhance flexibility and ductility. Therefore, with these unique observations future work can be developed; however, for this study graphite/graphene:acrylic composites were analyzed on its electrical and optical properties as a function of concentration and mechanical deformation.

CHAPTER 4: RESULTS AND DISCUSSION

4.1 Materials Characterization

As-received MoS_2 powder particles consisted of an original mean size of ~6.5 microns as seen in Figure 4.1, with a Nagakami probability distribution fit, which best fitted by Matlab software package.

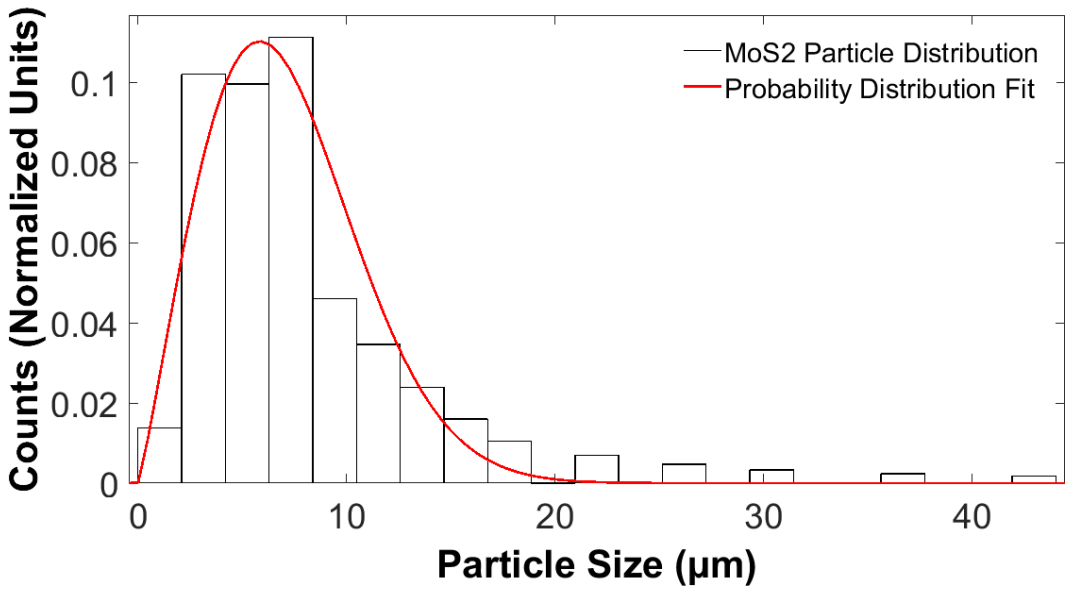

Figure 4.1 Measured as-received MoS_2 powder, with a Nagakami probability distribution fit.

Immediately after MoS_2 was subjected to ultra-sonication, the particles decrease in their size as a function of time; this shift to smaller particle sizes is shown in Figure 4.2. However, the fragmentation of particles did not take place at the same rate. The greatest particle size reduction with respect to time took place on the first interval of the ultra-sonication time during the first 30 min. Then, after 30 min, the reduction was not as pronounced as initially; however, the creation of a second mode and even a third mode at the 6-hour ultra-sonication time was produced. This generation of second and third modes shows a clearer change in particle size, in which they represent the transition between coarse to fine particles.

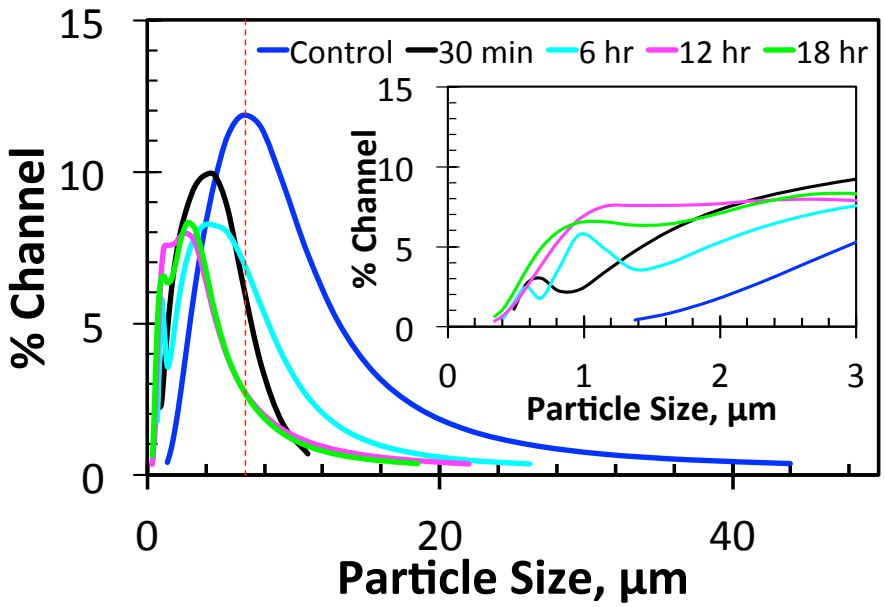

Figure 4.2 Particle size distribution of treated MoS_2 at different ultra-sonication times with an inset graph for finer MoS_2 particles.

This may suggest that as ultra-sonication time lapses at a constant power generation of new modes are developed in order to attain the smallest particle for that a particular power. Once the fragmentation of this particles lowers as a function of time, the particles will turn into a single mode.

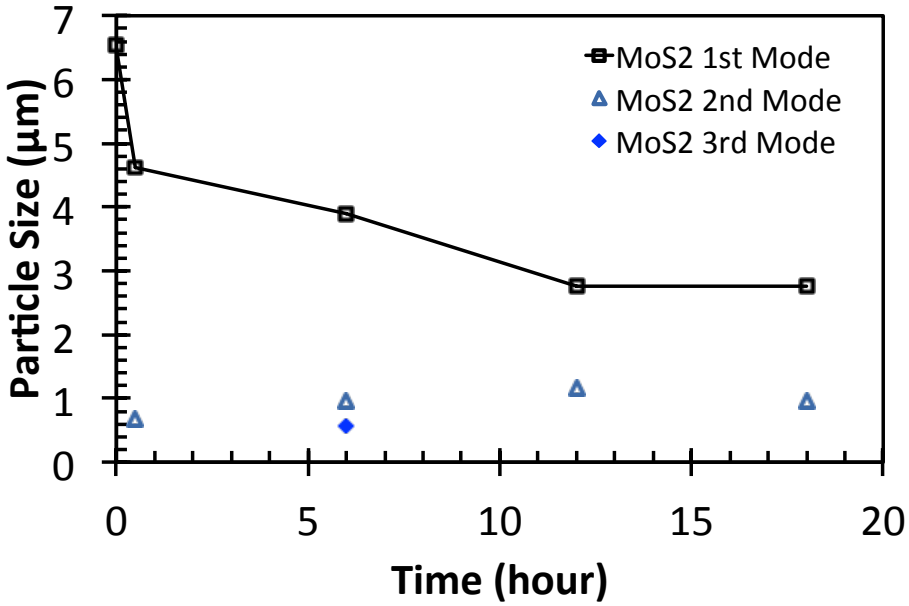

Figure 4.3 Particle size v. time graph of MoS_2 treated powder particles showing bi and tri-mode appearance.

In Figure 4.3 the generation of new modes are shown, and it can be seen how after 6 hours the third mode disappears and the second mode prevails even at 18 hour ultra-sonication time, which also suggest that if the powder was ultra-sonicated for longer times at the same constant power the second mode would have disappeared and the mean value of the single mode would have been ~1 micron size particle. In order words, it is suggested that at times longer than 18 hours the powder particle would eventually complete the transition to fine particles suitable for the operating power of the ultra-sonication system.

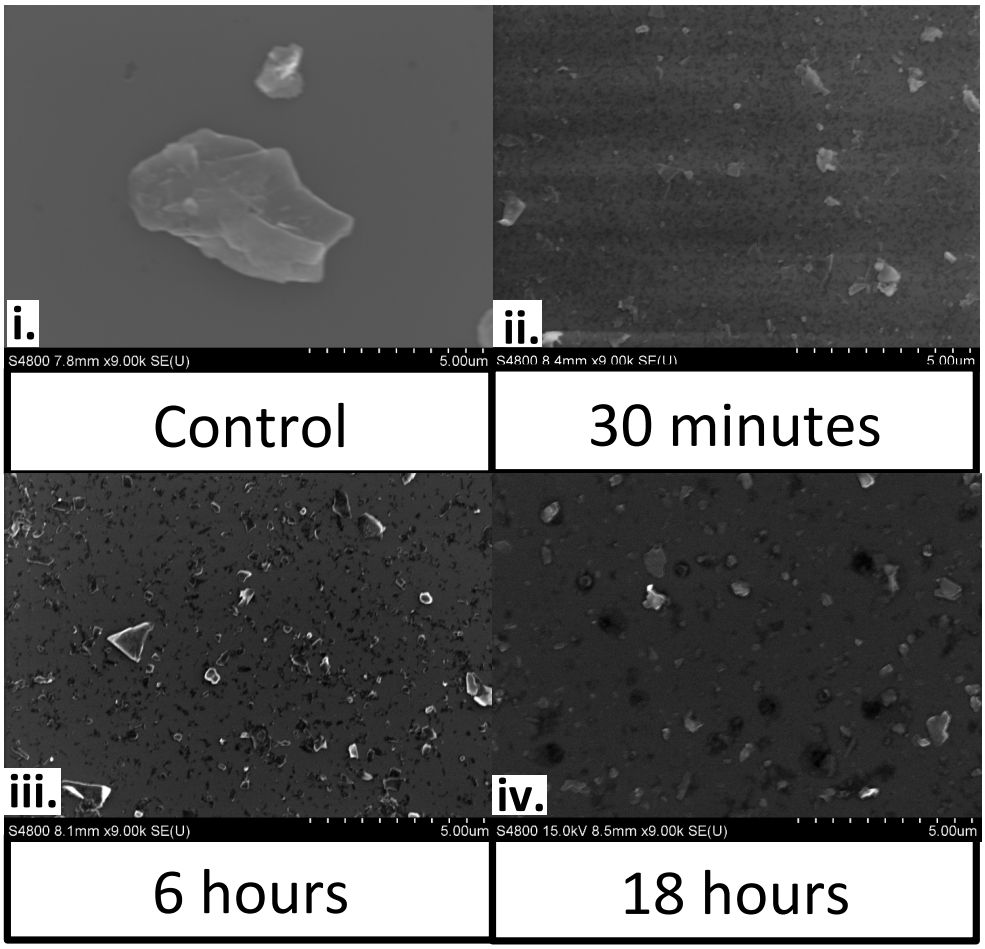

Figure 4.4 SEM micrographs of treated MoS_2 powder showing more particle dispersion as time increases with fine particles.

Then, in Figure 4.4, Scanning Electron Microscopy (SEM) effectively shows the change in particle size at 30-minute ultra sonication, where some coarse particles (charged in white) are shown as well as the finer particles. This background continued appearing at the 12 and 18 hours. More

specifically, the particles with triangle crystal flakes, which are signatures of exfoliated layer material. Consequently, due to the crystal-like flakes, Raman Spectroscopy confirmed in Figure 4.5 that after 18 hours of ultra sonication particles show $\Delta k=A_{1g}-E_{2g}=22.85cm^{-1}$, which there is between 2-3 MoS_2 layer flakes. Even though the particle fragmentation did not change substantially after 12 hours, shear forces acting on the particles produced possible 2-3 layer flakes. In other words, 18-hour ultra-sonication sample generated possible exfoliated MoS_2.

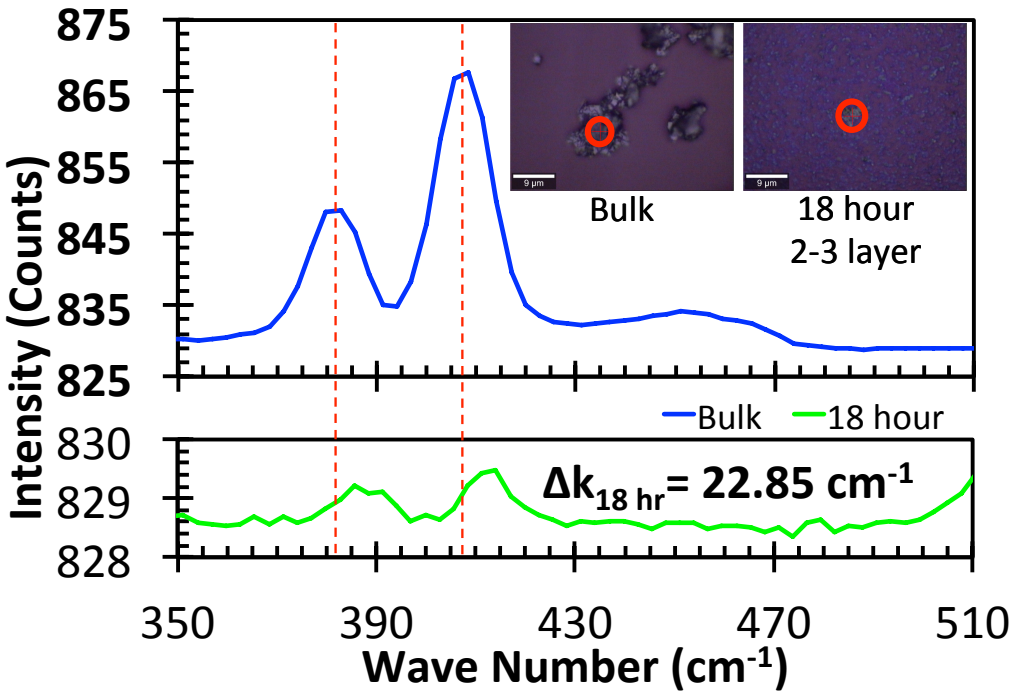

Figure 4.5 Raman Spectroscopy spectra of 18-hour and non ultra-sonicated treated MoS_2 powder with optical micrographs of measured regions.

However, there were also regions in samples with ultra-sonication times from 30 minutes, 6, 12, and even 18 hours were identifiable crystals seem to show typical MoS_2 features. Some other studies with similar ultra-sonication times but lower concentrations confirmed presence of exfoliated materials with no more than 4 layer structure (Yu et al. 2013).

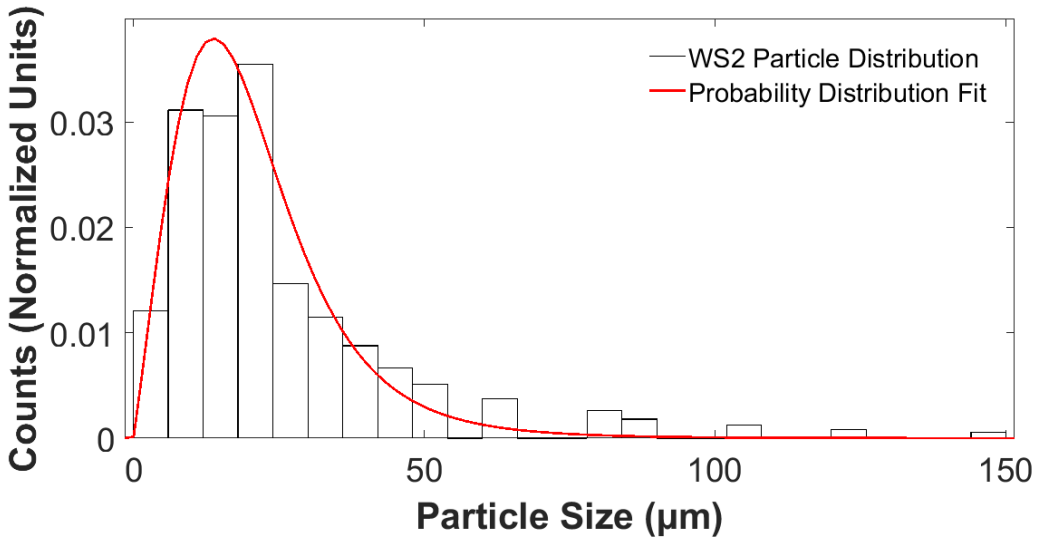

Figure 4.6 Measured as-received WS_2 powder, with a Burr probability distribution fit.

In the case of WS_2, similar behavior was produced; nevertheless, different results were produced when searching for the presence of 2D layer materials. Starting with Figure 4.6, the as received WS_2 powder distribution provided particles with a mean size of ~29 microns with Burr probability distribution fit, different than MoS_2.

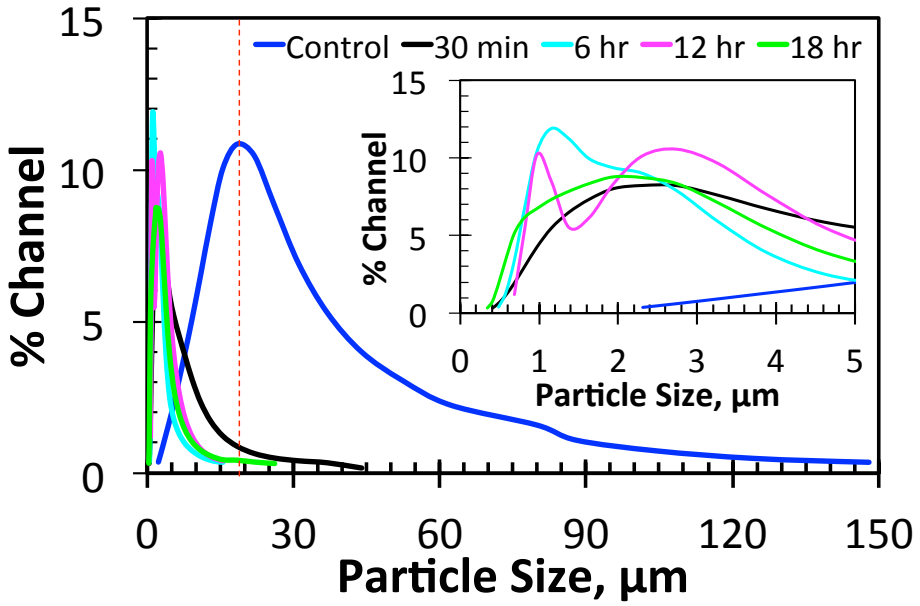

Figure 4.7 Particle size distribution of treated WS_2 at different ultra-sonication times with an inset graph for finer WS_2 particles.

Once exposed to the ultra-sonication experiment, the powder fragmentation increased rapidly for the initial 30 min, similar to MoS_2. After the 30 minutes of ultra-sonication, the distribution peaks shifted to the particle sizes between 3 to 1 μm as ultra sonication time increased. Compared to MoS_2, WS_2 did not produce any more significant changes in particles after the 30 minutes of ultra-sonication exposure. Even though the fragmentation was insignificant after the first measurement when the powder was exposed to agitation, WS_2 also was exposed to a bimodal distribution at 12 hours of ultra-sonication. This bimodal appearance, in which first and second mode peaks were closely together by 2 μm, was only present at that time of ultra-sonication because it vanished after 18 hours. This constitutes that even though the time increased and second modal appeared, the mean size of WS_2 particles remained in the same range. Because of the near proximity of both modes appeared at 12 hours and particle size reduction transition factors, bimodal presence did not last long enough. A clear transition can be shown in Figure 4.7, where the modal peak of the 18-hour sample relies in between of the bimodal peaks of the 12-hour sample measurement.

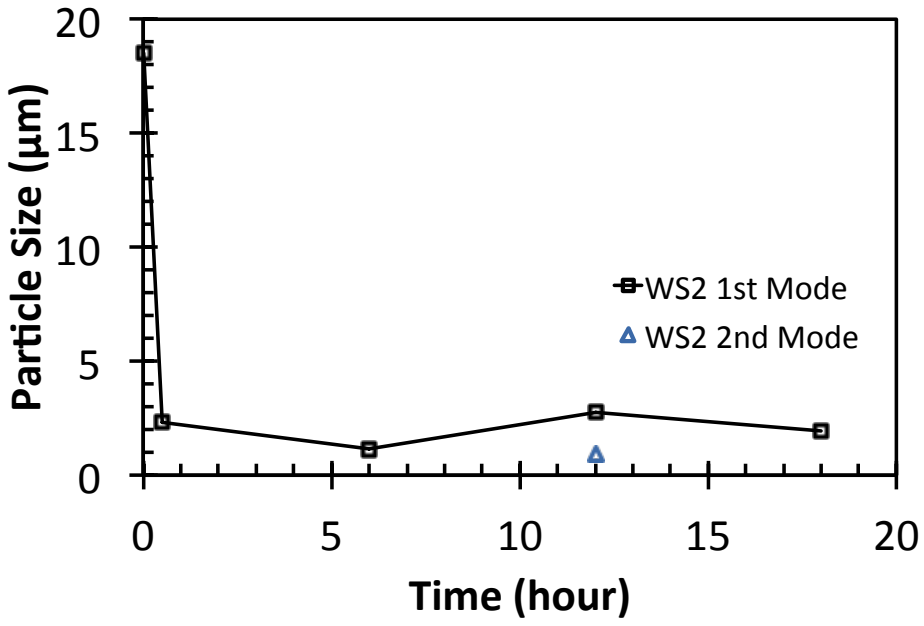

Figure 4.8 Particle size v. time graph of WS_2 treated powder particles showing bi-mode appearance.

It can be also possible that agglomeration of particles is taking place during Microtrac measurements, as the particles decreased in their size also the particles tend to agglomerated, making the Microtrac analyzer to measure a group of particles as a single particle.

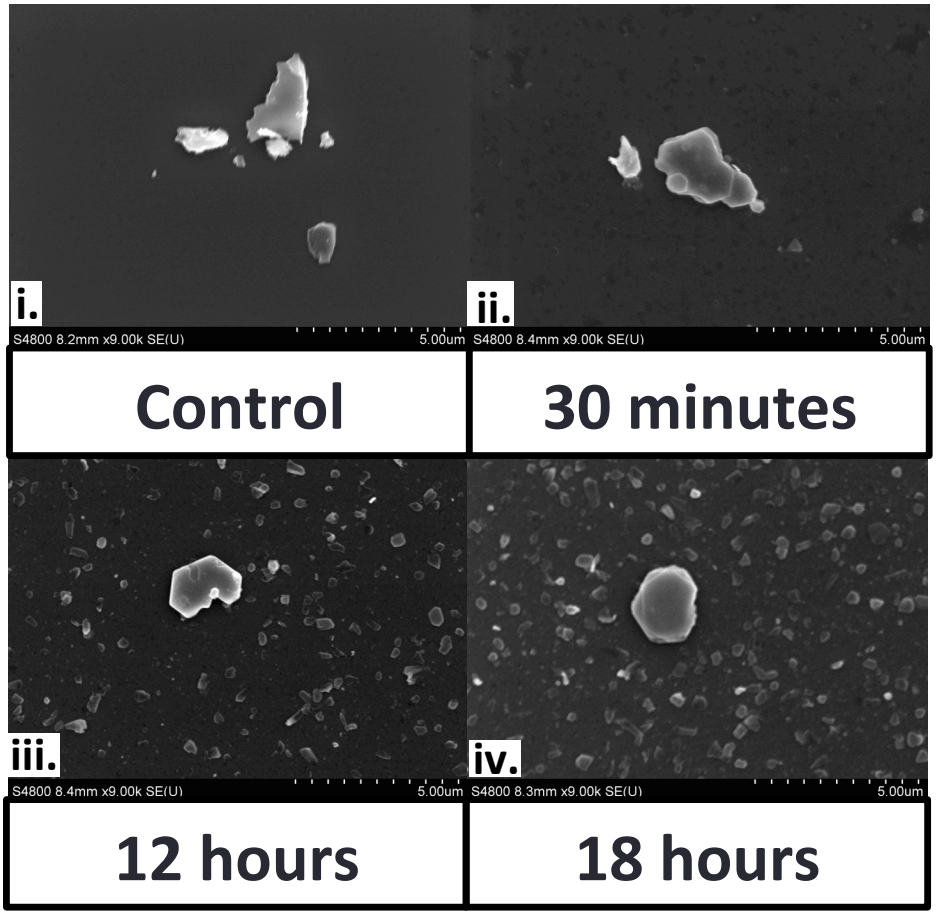

Figure 4.9 SEM micrographs of treated WS_2 powder showing more particle dispersion as time increases with fine particles.

Now, looking at the morphology of these WS_2 particles, Scanning Electron Microscopy showed clear signatures of crystalline structure with 120-degree hexagonal-like flakes, forming at the beginning, during the initial 30 minutes of the ultra-sonication. In Figure 4.9, the particle shape and size reduction can be seen at the different ultra-sonicated samples. Besides the particle reduction in Figure 13.iii and iv, the micrographs' background area is filled by the fine particles ultra-sonicated for 12 and 18 hours. There were some other regions in which less-crystalline structures were found. Therefore, this less-

crystalline (or non-120-degree shape) and the high-crystalline structures were compared in Raman Spectroscopy to identify any possible WS_2 layered material.

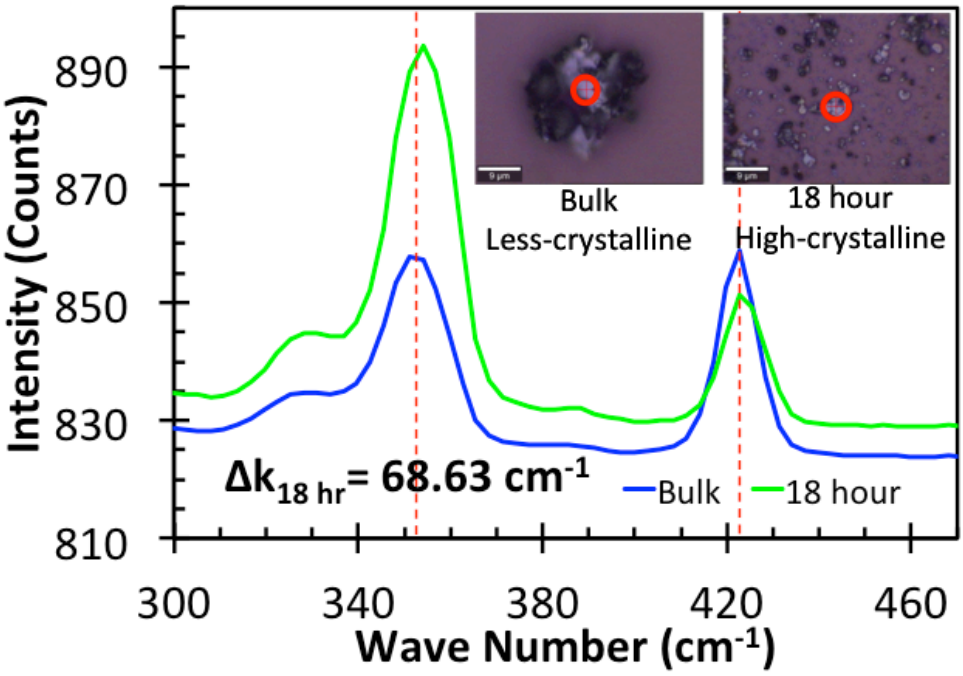

Figure 4.10 Raman Spectroscopy spectra of 18-hour and non ultra-sonicated treated WS_2 powder with optical micrographs of measured regions.

Raman Spectroscopy measured Δk_{18hr}=68.63 cm^{-1}, which is a value really close to the less-crystalline particle. In Figure 4.10, Raman spectra is shown and less-crystalline spectrum was superimposed onto the 18 hour sample with high-crystalline structure, so by looking at the Δk value of the high-crystalline particle or at the Raman shift between both spectra, there is negligible differences. Even though promising crystalline structures were clear signatures of 2D layer materials, unfortunately Raman measurements suggested and confirmed that there were no indicatives of such layer structures, but bulk material. There are also other studies in which the WS_2 was successfully exfoliated in NMP solution, but in that case concentration of WS_2 was lower than the one use in this study (Cunningham et al. 2012). Therefore, in order to carry out successful exfoliation of this material, concentration can be lowered or power at which this ultrasonic experiment can be increase to produce the necessary shear force to break-up the van der Waals bonds in the compound.

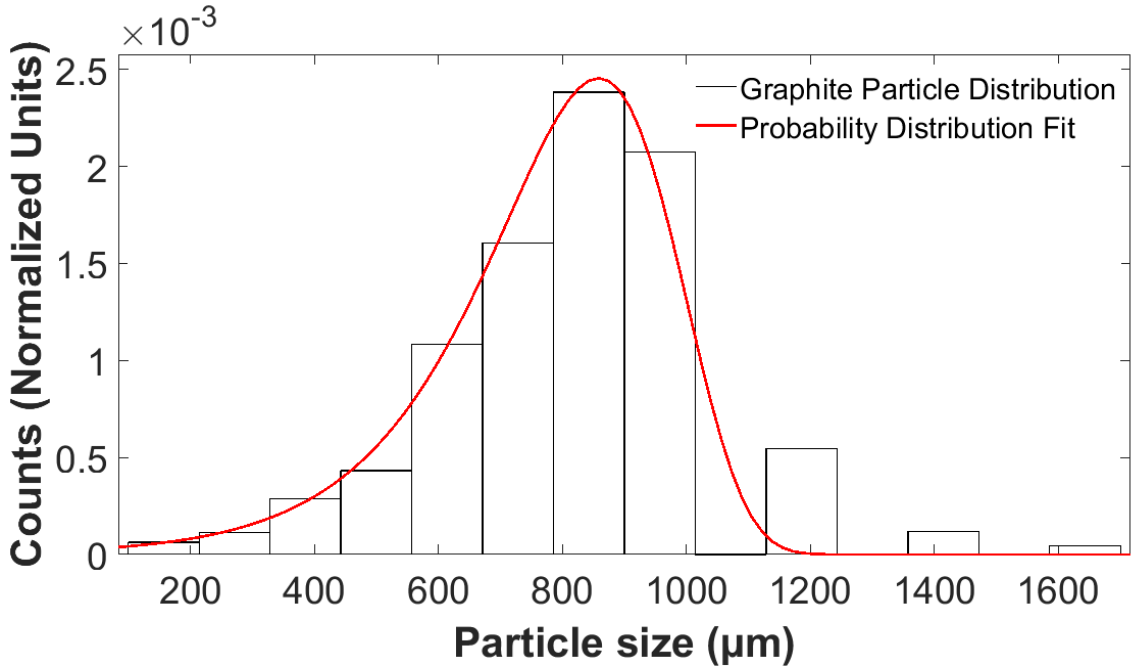

Figure 4.11 Measured as-received graphite powder, with an Extreme Value probability distribution fit.

Graphite particles in Figure 4.11, with a mean value of ~850 microns with Extreme Value probability distribution fit, were also exposed to ultra-sonication at the same times as the latter TMDCs materials. The graphite powder was considerably coarse, and as a result, the initial ultra sonication time shifted the distribution by ~73% reduction of its original size in Figure 4.12. Even though the highest fragmentation phase was between the control and the 30 minutes of ultra sonication, going from ~820 µm to ~225µm, the distribution in Figure 16 for the 30 minute ultra-sonication sample also generated a bimodal distribution. Once this particle size reduction took place, the graphite particles remained in the same range for both modes until it reached the 6 hours of ultra-sonication. After 6 hours of ultra-sonication the graphite particles were also participants of a new reduction in size, which can be shown in Figure 4.12 when looking at the 6 and 12 hours of ultra-sonication where the particles became one single mode distribution, with mean size of ~6 µm. With all the sample measurement shown in Figure 4.12 there are distinct shifts to the left, favorable to the decrease in particle size. Furthermore, in Figure 4.13,

it can be seen how the generation of new modal facets corresponds to the pronounced transition in particle size, from ~825 µm to ~6 µm.

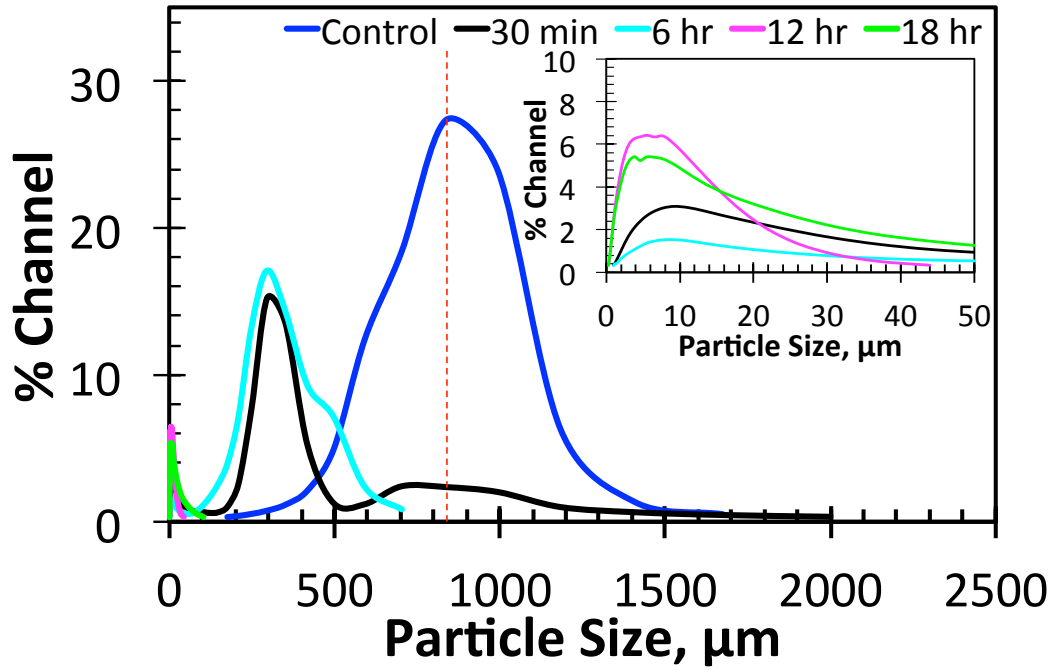

Figure 4.12 Particle size distribution of treated graphite at different ultra-sonication times with an inset graph for finer graphite particles.

The bimodal appearance, in the case of graphite powder, is shown at the platonic region in which no changes are produced in particle size. Once the powder fragmentation rate increases after the 12 hours of ultra-sonication the bimodal appearance disappears to generate the transition from coarse to fine particles. It is suggested that during ultra-sonication the smallest particle, possible for the operating constant power, was attained when 12-hour ultra-sonication finished with fine particles of ~6 microns and no bimodal distribution. These particles close to 6 µm and particles ultra-sonicated at the different times were also characterized by Raman Spectroscopy measurements. Even though about half of the identifiable crystals showed typical bulk graphitic features, the presence of possible mono to few layer graphene was also recognized, which can be developed and functionalized in a polymer composite matrix.

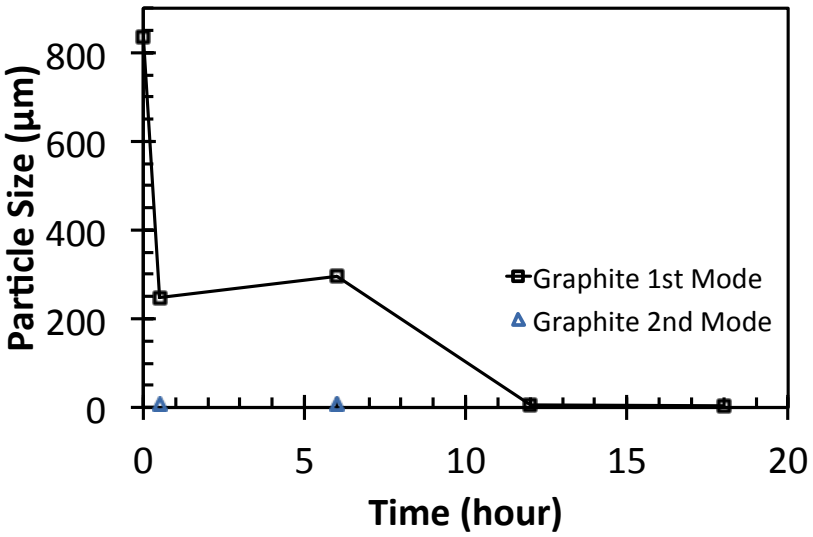

Figure 4.13 Particle size v. time graph of graphite treated powder particles showing bi -mode appearance.

Figure 4.14 shows the Raman spectra of a bulk and the few layer graphene structure in which Δk_{18hr}=1108.99 cm^{-1}, but most important I_{2D}/I_G>2, being a clear signature of few layer graphene structure. When compared this results with previous findings it can be confirmed the presence of few-layer graphite structure, where there have been shifts in the 2D peak, which is a determining factor for existence of few-layered materials (Yu et al. 2013).

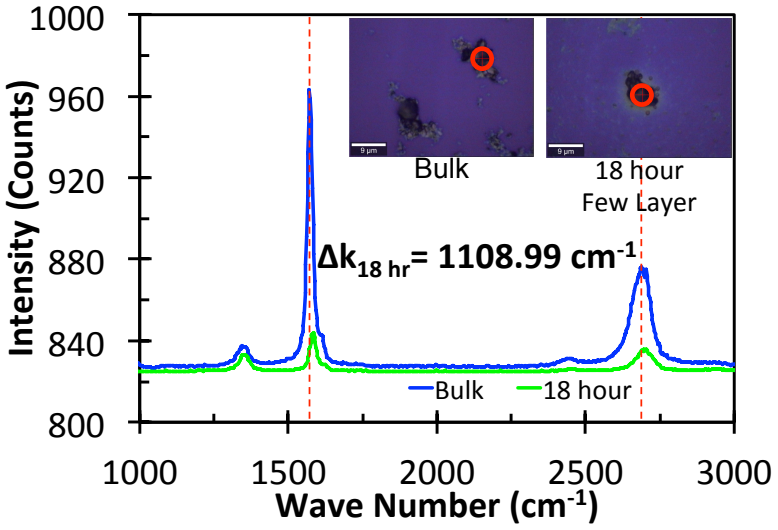

Figure 4.14 Raman Spectroscopy spectra of 18-hour and non ultra-sonicated treated graphite powder with optical micrographs of measured regions.

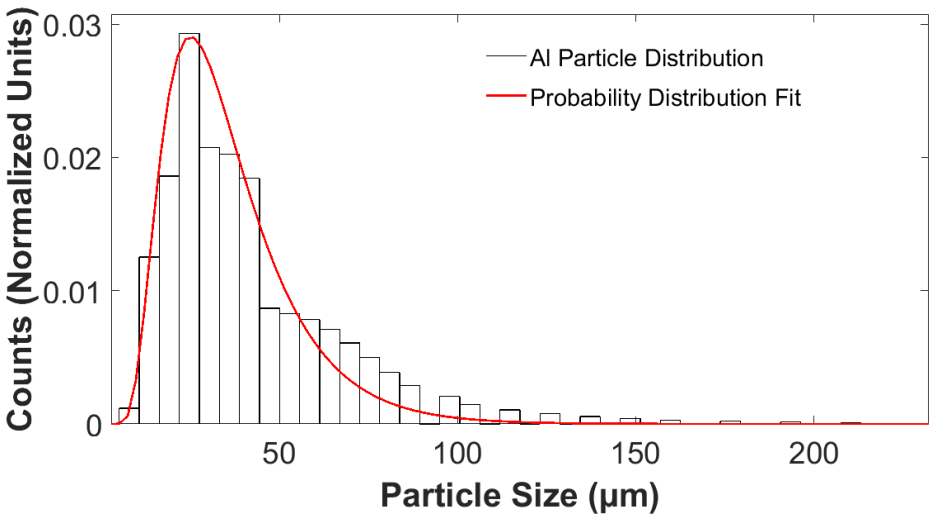

Figure 4.15 Measured as-received Al powder, with a Birnbaum Saunders probability distribution fit.

It is interesting to compare non-2D layered conductive materials with the TMDCs and graphene, from the very first stage of the experimental movement. The as received Aluminum powder consisted of Birnbaum Saunders probability distribution, shown in Figure 4.15, in which a clear distinction in the distribution was already notable as compared to the other treated materials.

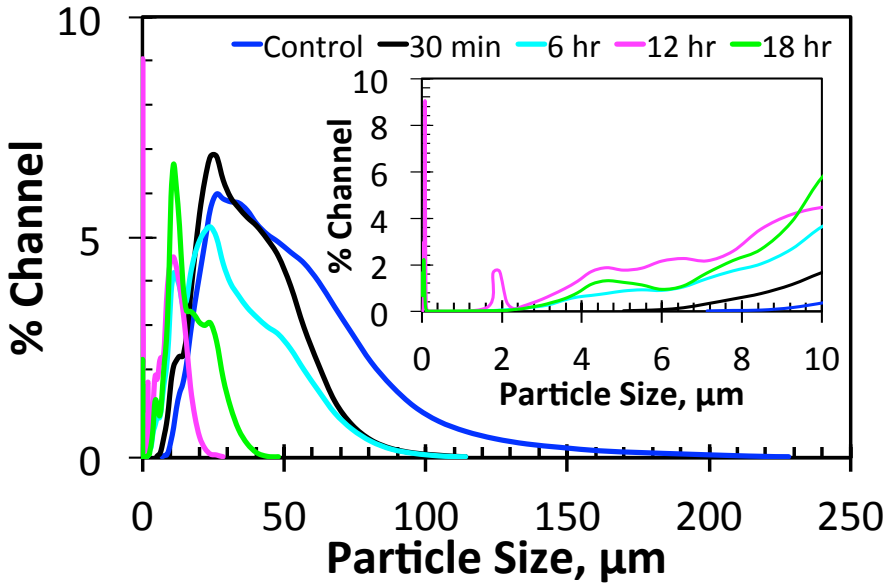

Figure 4.16 Particle size distribution of treated Al at different ultra-sonication times with an inset graph for finer Al particles.

After 30 minutes of ultra-sonication, there was not distribution shifts and a slightly change in the form of the distribution, shown in Figure 4.16, but no bimodal distribution was generated. It was not until 6-hour of ultra-sonication lapsed when fragmentation occurred; however, the Aluminum particles still coarse as compared to the particles shown in MoS_2, WS_2 and Graphite. Aluminum powder particles took 6 hours of ultra-sonication to achieve its highest fragmentation level, shown in Figure 4.17.

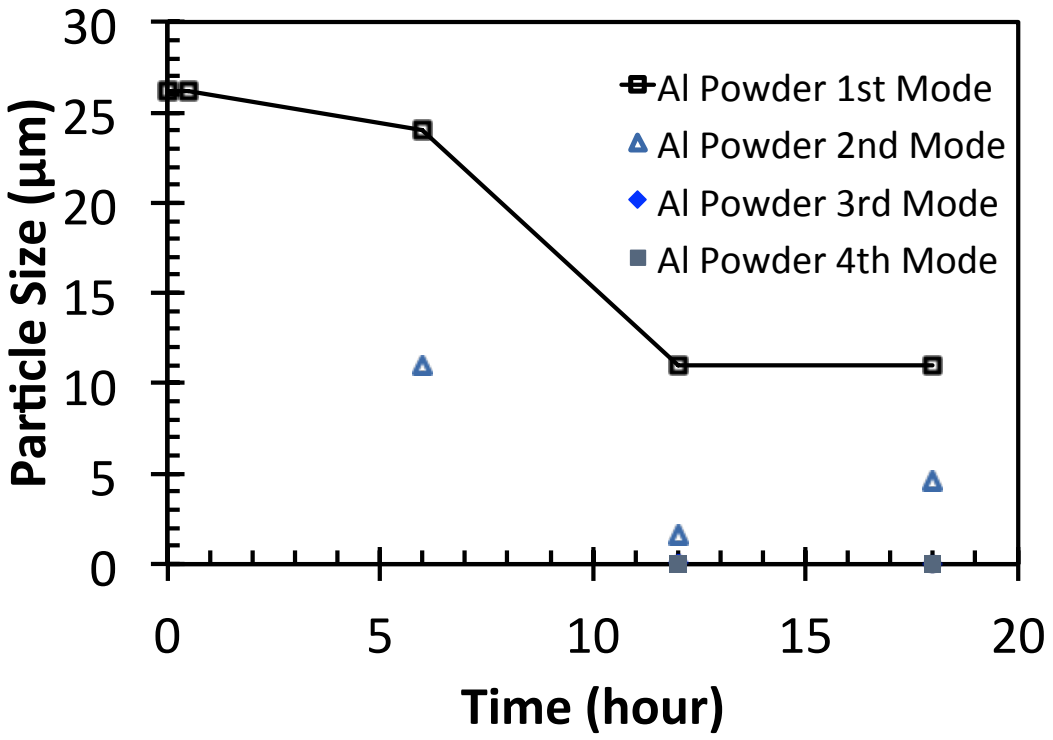

Figure 4.17 Particle size v. time graph of Al treated powder particles showing bi and tri-mode appearance.

This comparison between the metal, the TMDCs and graphite between 0 and 30 minutes of ultra sonication is provided in Figure 4.18 as the fragmentation rate (FR). Highest fragmentation rate is carried out by the graphite powder with -1176.4 µm hr^{-1} which had the highest initial particle size, the following was WS_2 with -32.4 µm hr^{-1} and also had the similar initial particle size as the Aluminum powder.

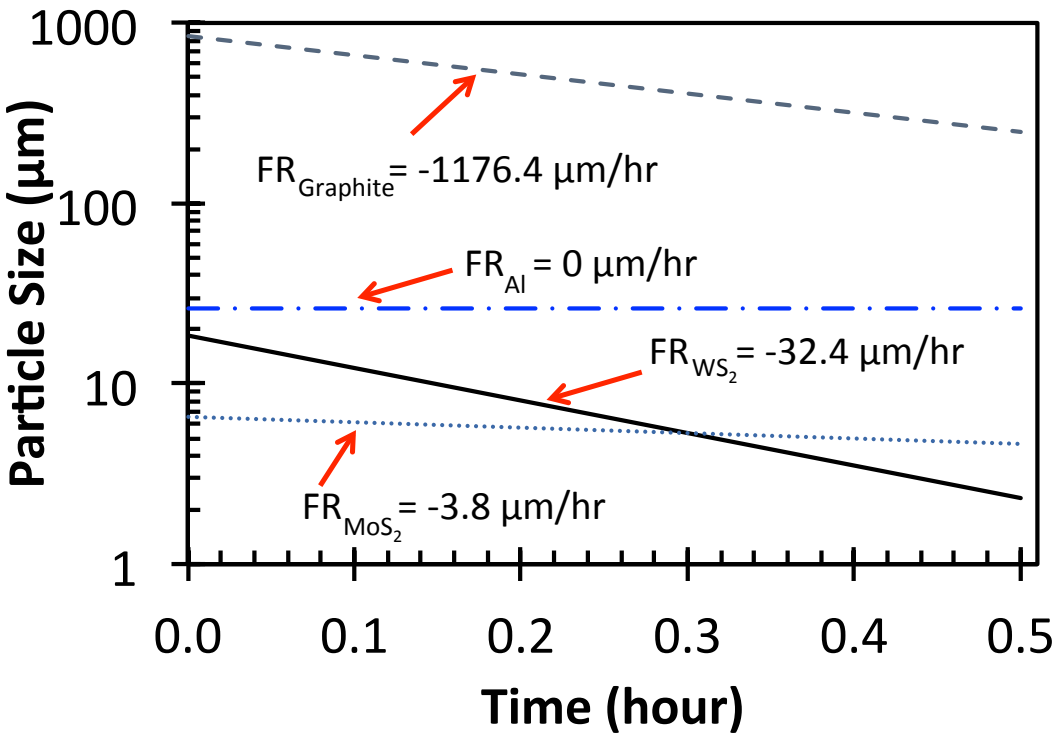

Figure 4.18 Particle Size v. Time plot showing Fragmentation Rate (FR) for all the treated powders at first interval of ultra-sonication.

Moreover, MoS_2 with the smallest initial particle size had a fragmentation rate of -3.8 µm hr^{-1}. Even though it was the lowest rate, MoS_2 attained the 2-3 layers. In the case of the Aluminum, the particles did not react the same in solution and in ultra-sonication such as the other materials; the fragmentation rate was 0 µm hr^{-1}, suggesting that metal properties with strong covalent bonds will resist to particle fragmentation at the initial 30 minutes of ultra-sonication.

As ultra sonication takes place, stresses are present and are induced into the particles. These induced stresses can act in compression or tension; as a result of these stress modes, the structure of any material would be compromised. Therefore, X-Ray Diffraction analysis provided measurements of these changes in crystalline structure, more specifically XRD provided with the changes in shift of the 2-theta angle due to the change in d-spacing of the 4 ultra-sonicated materials. In Figure 4.19 the XRD spectra of the different ultra sonication times is shown, and as seen through the particle measurement analysis the biggest fragmentation rate was at the initial 30 minutes of sonication; therefore, it would be

important to notice what was the behavior in terms of the shift in 2-theta. As expected, the greatest shift in 2-theta was obtained with the 30 minute ultra-sonicated sample, in which both TMDCs and Graphite show relative similar shifts in the compressive side, whereas in the case of the Aluminum powder the shift is negligible. Therefore, similar behavior for 2D layered materials is seen when exposing them into ultra-sonication in NMP solution for 30 minutes. Now, after subjecting the samples to 18 hours of ultra-sonication, TMDCs and graphite took a different paths, in which the change in 2-theta in TMDCs was reduced and shifted to right side on their tensile side. It was not the case for the graphite in which it was reduced a minute fraction and remained in the same compressive direction. On the other hand, Aluminum powder experienced a completely opposite behavior as the TMDCs, in which Aluminum after 18 hours of ultra sonication the 2-theta peaks shifted from the negligible tensile direction to a considerable shift of 10-degrees in the compressive direction.

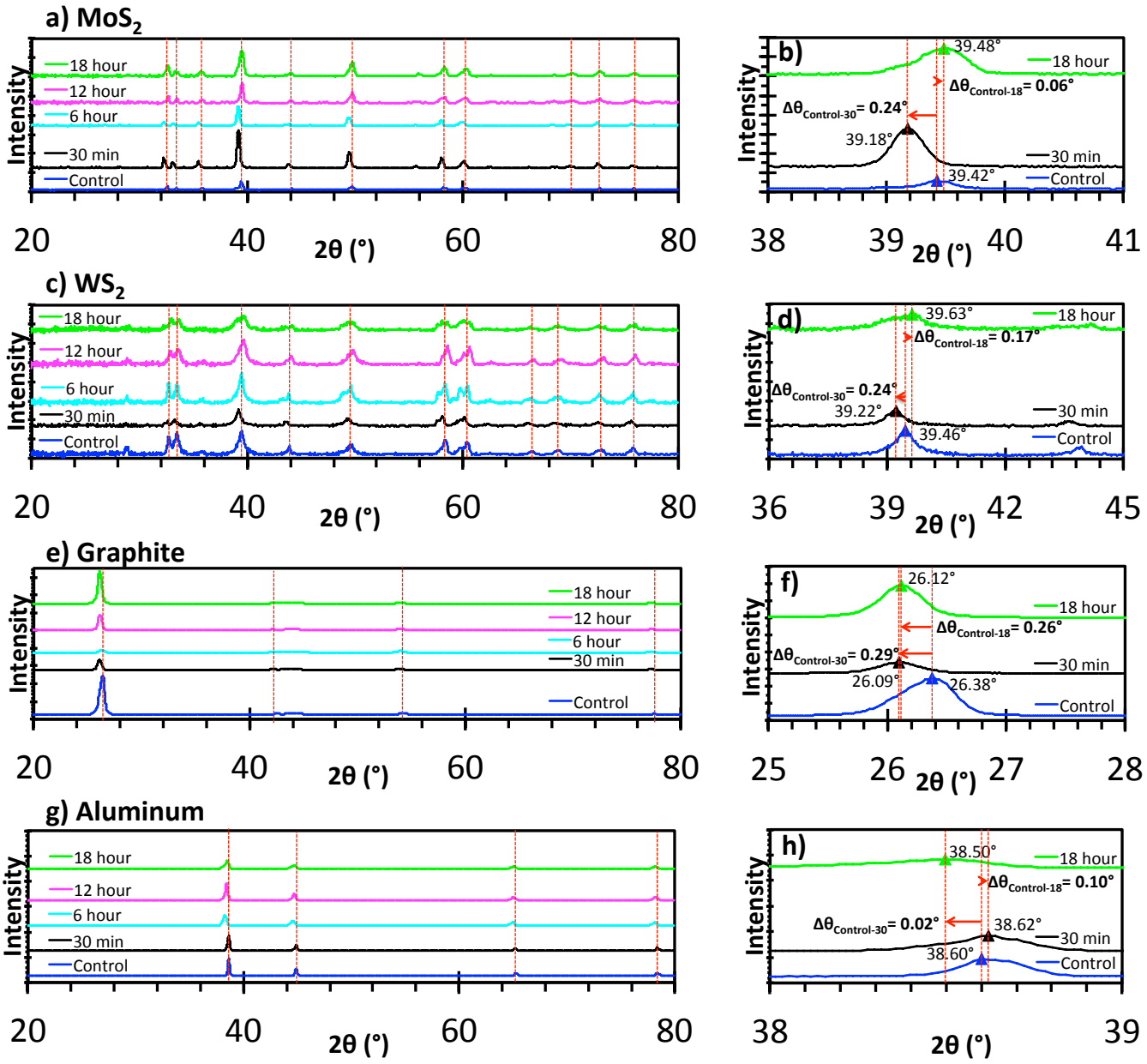

Figure 4.19 Complete X-Ray Diffraction spectra for a control sample and ultra-sonicated powders treated at 5 different times (left). XRD spectra showing the direction and change in 2-theta of a single peak at 30 minutes and 18 hours of ultra-sonication (right).

4.2 Hybrid Composite Characterization

4.4.1 Optical Measurements

When the acrylic was subjected to the different radii of curvature, Cary 5000 was utilized to measure optical absorption. When the composite is mechanically deformed as a function of radius of curvature, there are two modes that should be considered; the first one is on the top surface of the

composite, which is in tension and the second is the lower surface being compression. When tension dominates in the deformation, particles separate from one another and absorption is lower. Now, if the compression mode is the leading deformation mechanism, particles will shorten their distance between one another and absorption will increase.

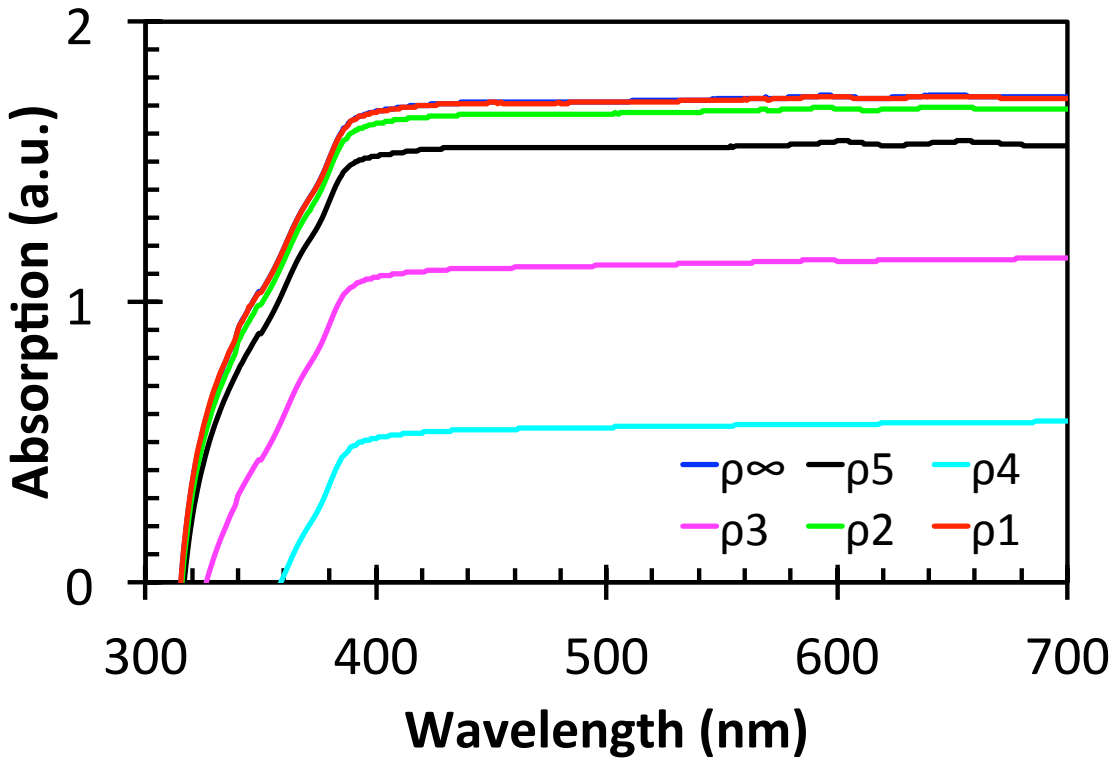

Figure 4.20 Absorption spectra of graphite/graphene:acrylic composite at 250 mg mL^{-1} of graphite/graphene concentration for the 6 radius of curvature.

In Figure 4.20, the optical measurements are shown for the 250 mg mL^{-1} concentration of graphene, which shows a comparison between the radii of curvature, in which for ρ_5 and ρ_4 the absorption decreases, meaning there is a tensile dependence, but once it goes to higher radius of curvature, compression dominates and absorption increases again. This trend is also replicated in figure 4.21 in line GP 300 mg mL^{-1} at 550 nm in wavelength, in which the lowest absorption measurement was when bending the composite to ρ_4. Then, for higher concentrations of graphene in the acrylic the response to optical absorption was not sensitive.

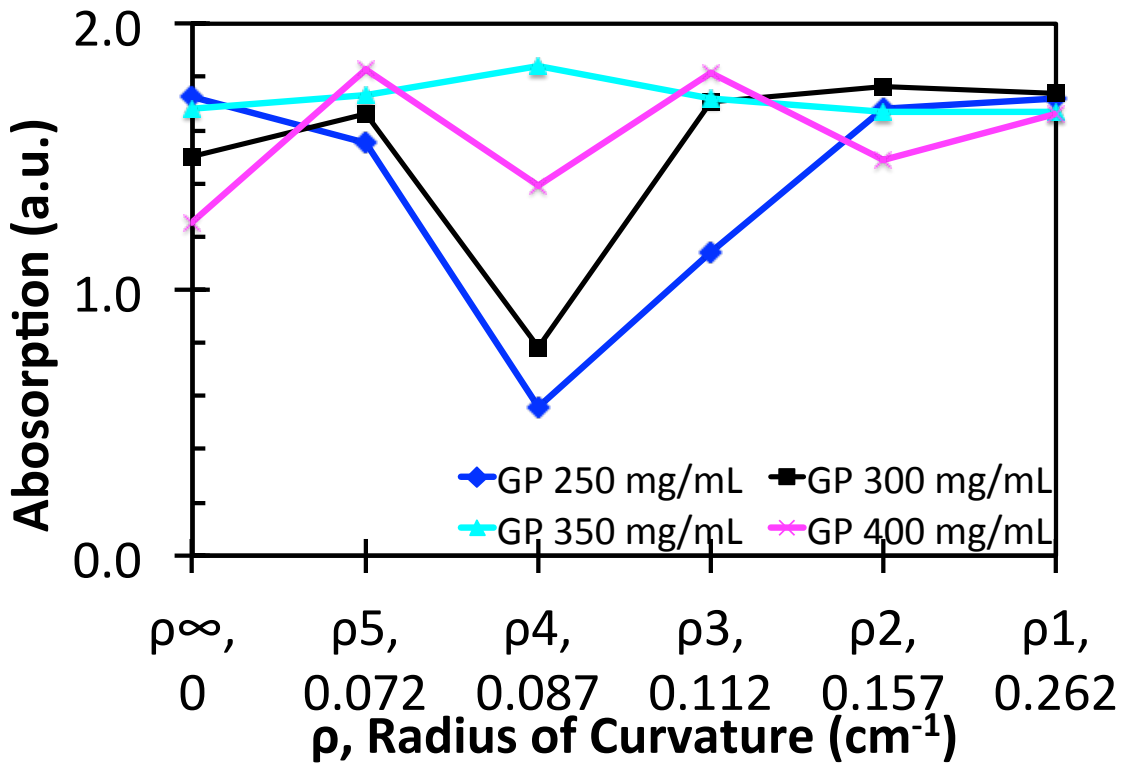

Figure 4.21 Absorption v. radius of curvature plot at 550 nm for graphite/graphene:acrylic composite for all graphite/graphene concentration.

4.2.2 Electrical Properties

Using the same radius of curvature fixtures as in the optical measurements for the acrylic composite, electrical data was also measured, and in Figures 4.22-4.25 all the measurements at different graphite/graphene concentrations can be seen. The behavior of the acrylic composites at different concentrations achieved a set point between 300 mg mL^{-1} and 350 mg mL^{-1}, in which the I-V response proceeded with distinctive behavior in 250 and 300 mg mL^{-1} in contrast with the composites with 350 mg mL^{-1} and 400 mg mL^{-1}. It is well understood from Balberg et al that percolation theory is present in conductive composites materials and that the there is a contribution of the non-nearest particles causing tunneling effect. Their study suggested that there is a threshold percolation, in which the particles on the matrix are not only connected electrically, but also are connected by the physical geometry of the particles in clusters, or agglomerated particle (Balberg et al. 2004).

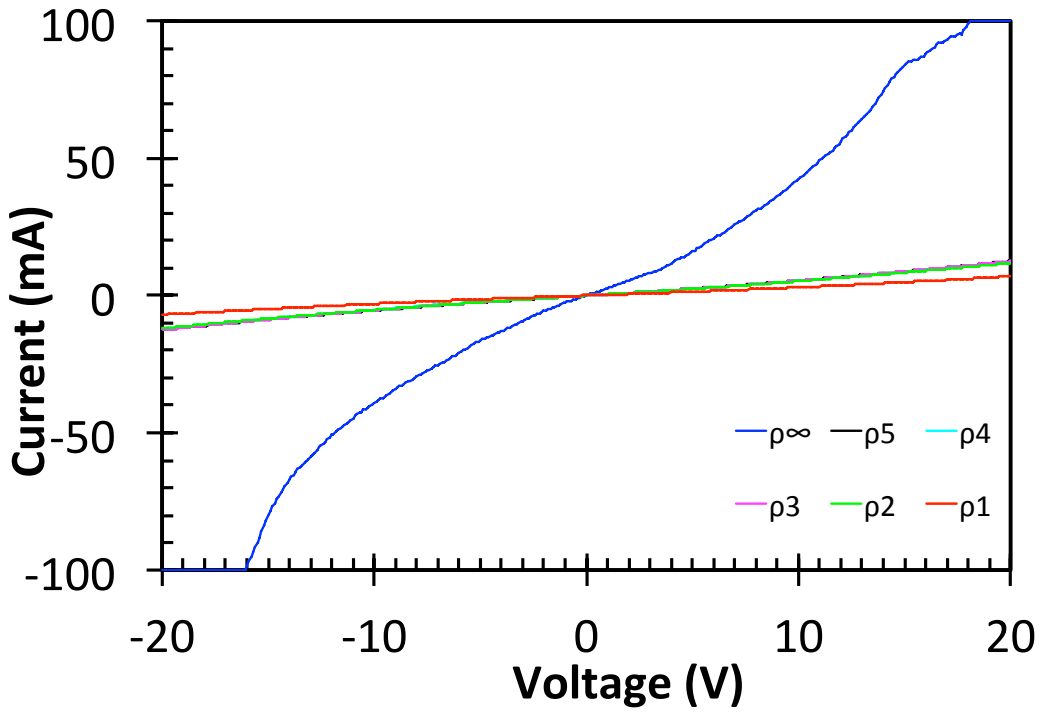

Figure 4.22 I-V response of graphite/graphene:acrylic composite with 250 mg mL^{-1} of graphite/graphene concentration at 6 radius of curvature.

In the created acrylic composites at the different graphite/graphene concentrations, the samples seem to reach the percolation threshold. However, this percolation threshold it is reached at different points of the I-V response, as a function of the graphite/graphene concentration and the radius of curvature while bending the sample. In the case of Figure 4.22 the initial I-V response is trailed by the non-nearest particles, in which percolation is not dominating the current flow; therefore, the non-ohmic response is seen at ρ_{∞}. The non-ohmic reaction, caused by tunneling effect, started ceasing and percolation theory initiated dominance right after the 250 mg mL^{-1} samples was exposed to elastic deformation at ρ_5. The acrylic composite sample with 300 mg mL^{-1} in Figure 4.23 showed a similar pattern as Figure 26, tunneling effect guided electrons with less resistance; however, in this samples the non-ohmic form at $\rho\infty$ was not as pronounced as the sample with lower graphite/graphene concentration. But a particular response appeared at ρ_4, which came up to be the curve with the most dominance of percolation theory, even though the non-ohmic remained present at all I-V measurements with respect to

the bending deformation. At this point, the two lower concentrations showed a behavior where tunneling effect is present at all times, but it is more evident as the radius of curvature decreases.

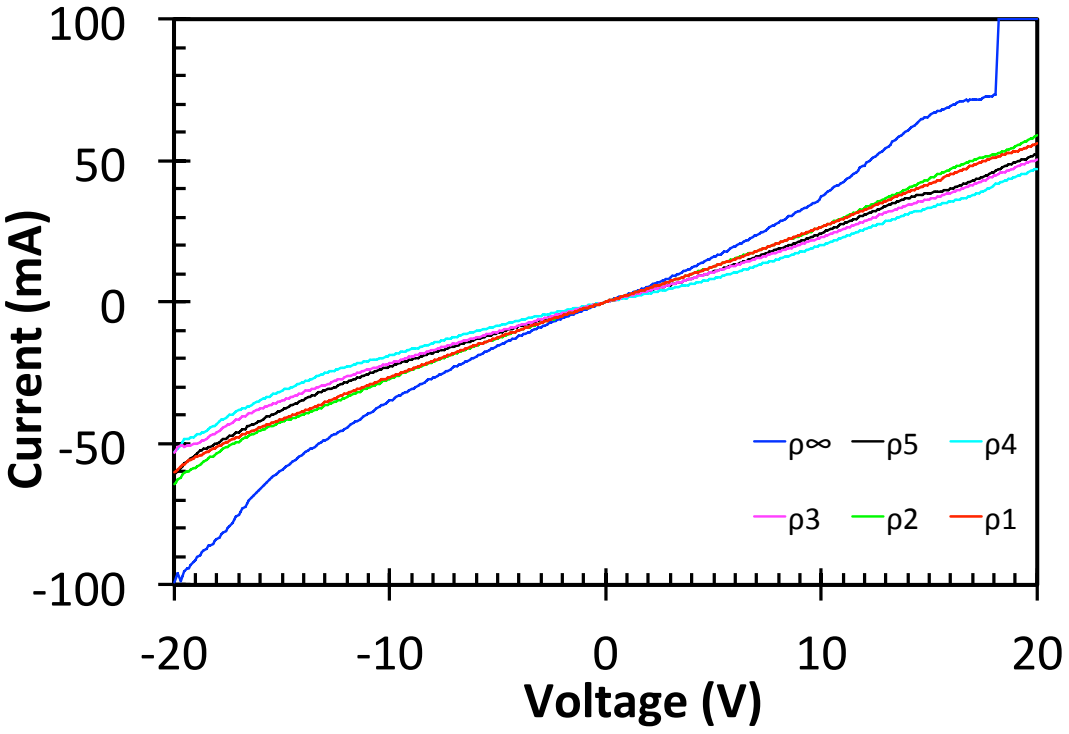

Figure 4.23 I-V response of graphite/graphene:acrylic composite with mg mL^{-1} of graphite/graphene concentration at 6 radius of curvature.

Furthermore, in the relatively higher graphite/graphene concentration acrylic composites, the configuration was completely contradictory. In Figure 28, 350 mg mL^{-1} sample, a transition happens in which the percolation theory appears controlling current flow at ρ_0. This different response clearly identified a set point in which particles are agglomerating more and facilitates the increments in current. Even though this new behavior for this composite appeared to dominate since the beginning of the I-V measurements, surprisingly, the non-ohmic started to be more pronounced ρ increased. This behavior, unlike the lower concentration samples, produced a tunneling effect to be more effective path than the percolation theory.

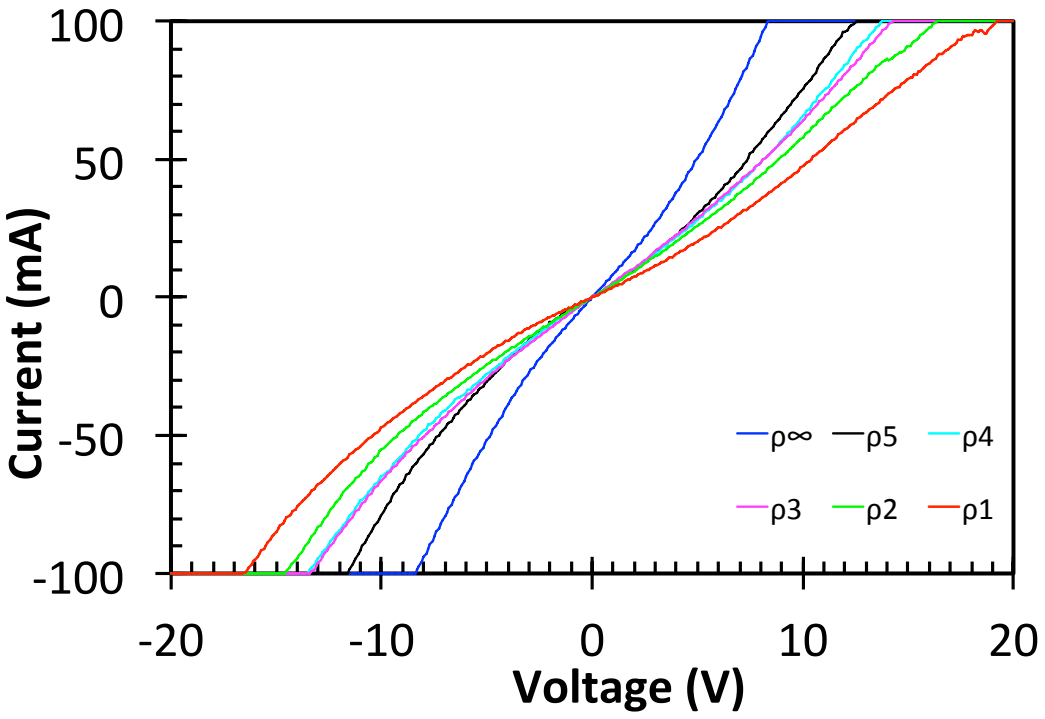

Figure 4.24 I-V response of graphite/graphene:acrylic composite with 350 mg mL^{-1} of graphite/graphene concentration at 6 radius of curvature.

Finally, in Figure 4.25, the percolation threshold has been achieved by the samples with 400 mg mL-1 graphite/graphene concentration. At ρ_∞ the I-V response reaches linear, ohmic response, but once more as ρ started to increase the non-ohmic curve began to emerge. These responses from the different samples opens the discussion of why the lower concentrations produced non-ohmic to ohmic transition as ρ increased, as the higher concentration samples developing a ohmic to non-ohmic response. The answer to this question needs to consider the modes acting on the samples as a function of bending. As the optical measurements, tensile and compressive modes became a part for suggesting analysis on absorption acquisition; it is assumed that as ρ increases the shortest path that current flow can take is through the compressive mode. Therefore, during this mode the distance between particles is much smaller; this means that nearest neighbor particles lowers the resistance of current flow by creating the shortest path at that radius of curvature. It is assumed then that clusters of particles are close enough to

follow percolation theory. This approach or assumption can be understood at the lower concentrations in which non-ohmic attempts to reach an ohmic linearity.

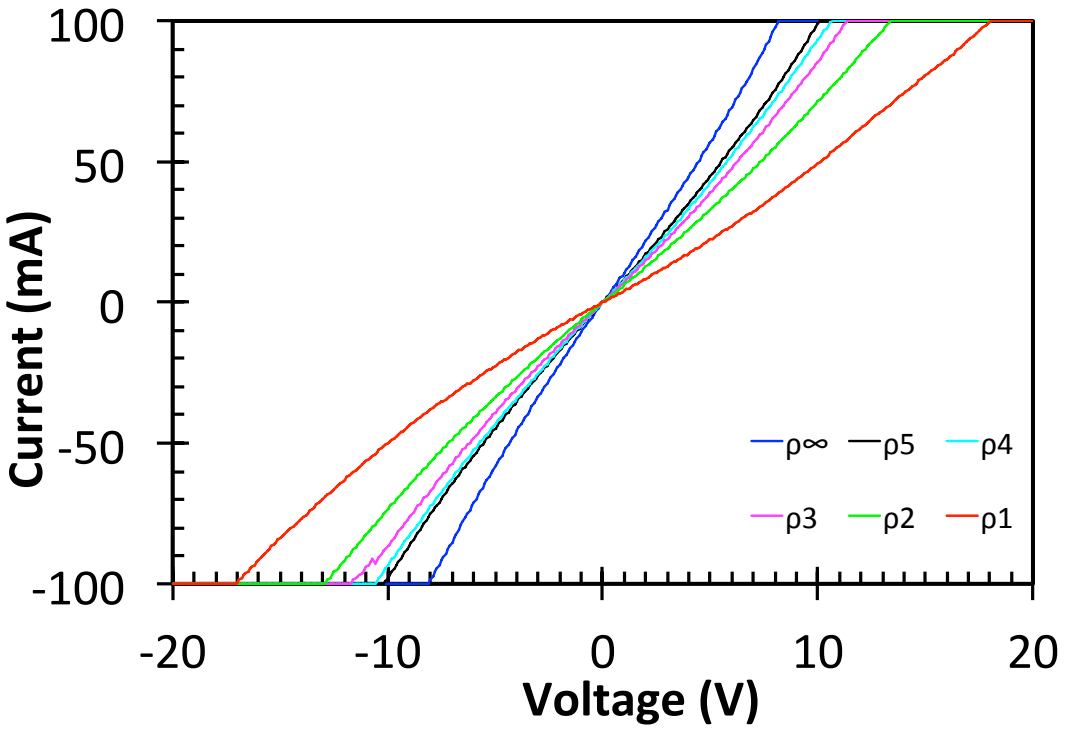

Figure 4.25 I-V response of graphite/graphene:acrylic composite with 400 mg mL^{-1} of graphite/graphene concentration at 6 radius of curvature.

On the other hand, the higher concentration samples did not recognize the compressive mode as the lowest resistance path. Consequently, as the radius of curvature increases the non-ohmic reaction shows to be more remarkable, which means that conductivity stops following percolation theory and tunneling effect dominates the current flow. At higher graphite/graphite concentrations the current flow is dominated by the tensile mode, in which particle distance increase as a function of radius of curvature. While the deformation is increasing the current flow finds the further nearest particles, connected electronically, but not physically, the path with less resistance. Both assumptions have to be considered to understand the behavior of these two sets of graphite/graphene concentration. The acrylic composites demonstrate to behave as a semiconducting material, in which quantum mechanics can dominate at depending on the concentration and the radius of curvature with tunneling effect, represented by the

non-ohmic behavior. The composites that were created showed sensitiveness of the percolation theory and tunneling effect at every sample upon deformation with respect to the radii of curvature, especially at the initial bending between ρ_∞ and ρ_5.

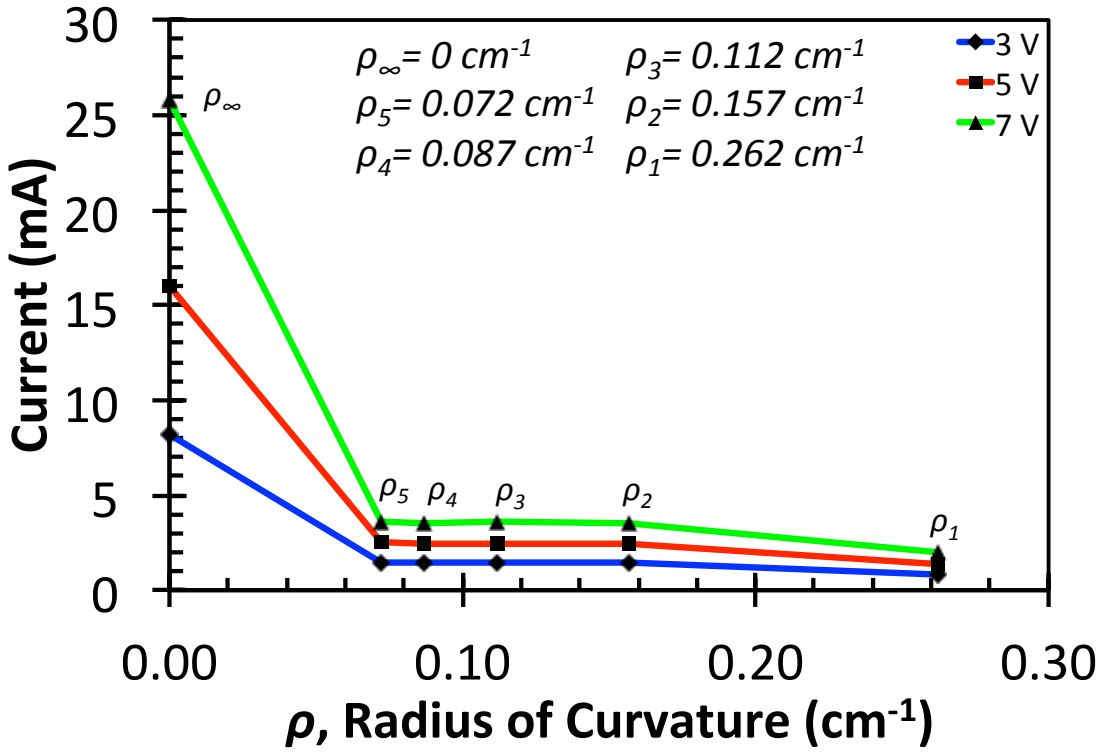

Figure 4.26 Current v. radius of curvature plot at 3, 5 and 7 V for graphite/graphene:acrylic composite at 250 mg mL^{-1} graphite/graphene concentration.

These four different graphite/graphene concentrations additionally produced changes in the current y-axis. The current was expected to increase as the concentration increased. Even though this was the case, the current always generated measurements in mA, only was exposed to one considerably change in current. As seen in Figure 4.26, 250 mg mL^{-1}, the initial current with no deformation was ~25 mA at 7V, then once the concentration was increased to 300 mg mL^{-1} there was no increment in current at ρ∞, but the current remain close to 25 mA at 7V, Figure 4.27. However, once the previous discussed threshold was achieved at 350 mg mL^{-1} the current increased substantially to ~80 mA at 7v, as seen in Figure 4.28, and it remained there for the next increment in concentration, Figure 4.29. Even at no deformation, the differences between low and high concentration are noted as the I-V responses explain

at the beginning of this section. Even though the concentrations play a big role in this impressive change in current, please note that tunneling effect and percolation theory decrease and increase the current flow, respectively. After reviewing this changes in current at 7V with no deformation taking place at ρ_∞, let us now consider the current flow as the deformation took place.

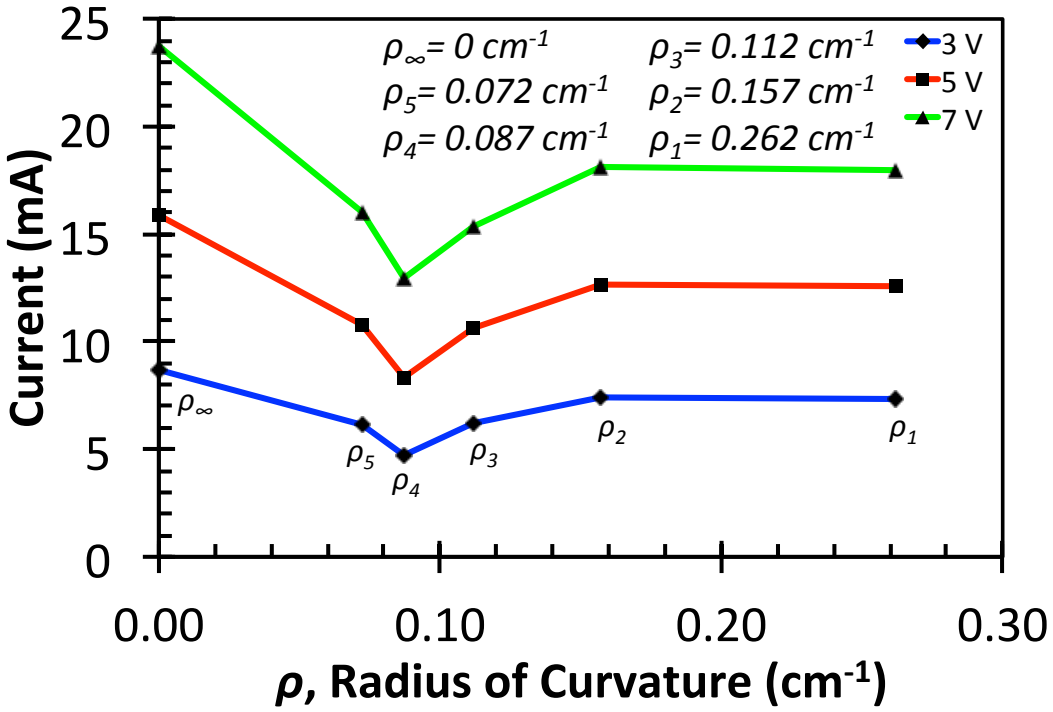

Figure 4.27 Current v. radius of curvature plot at 3, 5 and 7 V for graphite/graphene:acrylic composite at 300 mg mL^{-1} graphite/graphene concentration.

From ρ_∞ to ρ_5 all different concentration acrylic composite samples experienced the considerable values for current sensitiveness, which were calculated to be de following: 307.7 mA-cm for 250 mg mL^{-1}, -107.1 mA-cm for 300 mg mL^{-1}, -456.0 mA-cm for 350 mg mL^{-1}, and -250.9 mA-cm for 400 mg mL^{-1}. These current sensitivities suggest bringing suitable properties to strain sensing applications at this particular deformation. It was anticipated that a drop of current could be observed after increases in radius of curvature; however, this was not the only case detected. There were regions during I-V testing measurements in which current increased and sections where the current experimented minimum (neglecting) changes. While testing 250 mg mL^{-1} at greater ρ values, current decreases rapidly as seen in

Figure 4.26, where sensitivity decreased to 0 mA-cm from ρ_5 to ρ_2, and finally from ρ_2 to ρ_1 the sensitivity increased once more with minimum changes in current. In the case of the 300 mg mL^{-1} sample, the sensitivity was larger from ρ_5 to ρ_4 than from ρ_∞ to ρ_5, Figure 4.27. However, when subjecting the sample from ρ_4 to ρ_3, it was exposed to sensitiveness in the opposite direction, which was not expected, because this direction changed, generating an increment in current and continuing to increase until ρ_2 where no sensitivity was detected through ρ_1. It has to be noted that the same bending point, ρ_4, was the same point where the sample experienced a decrease in absorption discuss previously in Figure 4.21.

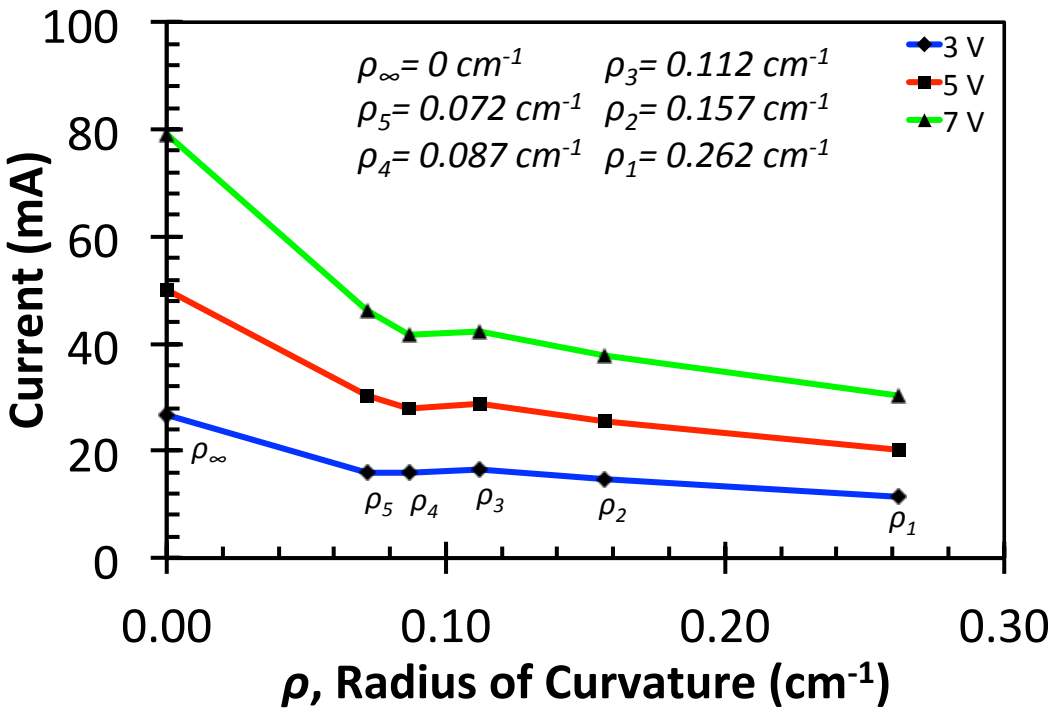

Figure 4.28 Current v. radius of curvature plot at 3, 5 and 7 V for graphite/graphene:acrylic composite at 350 mg mL^{-1} graphite/graphene concentration.

The increase in current can be explained by adopting the percolation theory, taking place as the bending increases, which is what was stipulated in the latter discussion on the modes affecting the I-V response. In 300 mg mL^{-1} sample the compressive mode is dominating the current flow as the elastic deformation increases; therefore, percolation theory facilitates the current flow rather than tunneling

effect where there is more resistance of the current flow. Explaining this, also confirms that the same thing is happening in the 250 mg mL^{-1} sample in which, as previously mentioned, there is no substantial decrease in current after the ρ_5, where percolation starts leading the response carried by the compressive mode. At the higher graphite/graphene concentrations, such as 350 mg mL^{-1}, the current drop appears to have similar effect as 250 mg mL^{-1} where from ρ_4 to ρ_3 the sensitivity is close to 0 mA-cm; yet, after ρ_3 the current keeps decreasing. On the other hand, in Figure 4.29, 400 mg mL^{-1} sample shows that current drops at every ρ value. In both cases higher resistances appeared as the deformation decreased, and knowing the change from I-V curve response, it is suggested that this can confirm the tension dominance at the higher concentrations where tunneling effect is more present than percolation theory. Since there is a relationship of electrical and optical as a function of its mechanical behavior, the composites discussed at this point can be set as optoelectronic and mechanical sensors using only the small values for ρ.

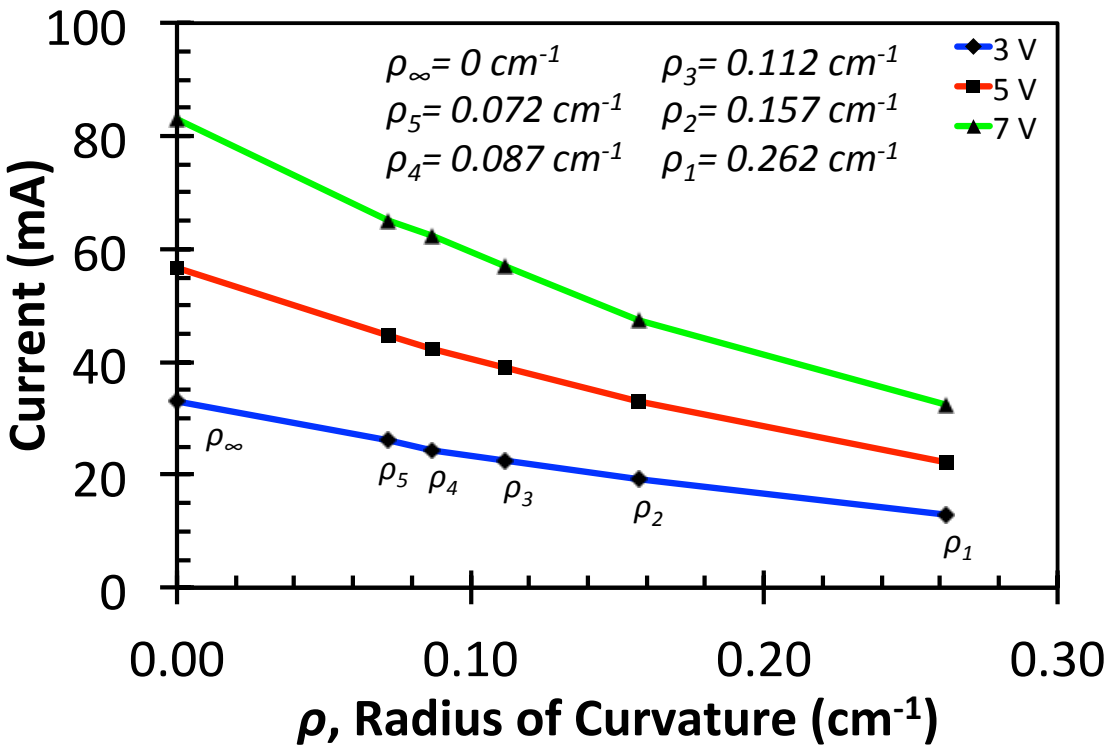

Figure 4.29 Current v. radius of curvature plot at 3, 5 and 7 V for graphite/graphene:acrylic composite at 400 mg mL^{-1} graphite/graphene concentration.

Once treated rubber bands were generated, only I-V measurements were performed, since there was no transparent baseline to provide accurate optical measurements. In Figure 4.30, the measurements of the treated rubber band for 37.5 mg mL^{-1} graphite/graphite concentration in NMP are shown. Unlike from the acrylic composites, the I-V response for both concentrations showed an ohmic behavior at all % strain measurements. In other words, each graphite/graphene rubber bands exhibited an ohmic behavior regardless the change of percent strain due to the tensile motion produced by the local-standardize tensile device. During the transportation if the graphite/graphene dispersed in an NMP:water solution. Both composites showed similar current with respect to voltage and % strain, only after 100% strain the difference becomes a greater due to higher concentration.

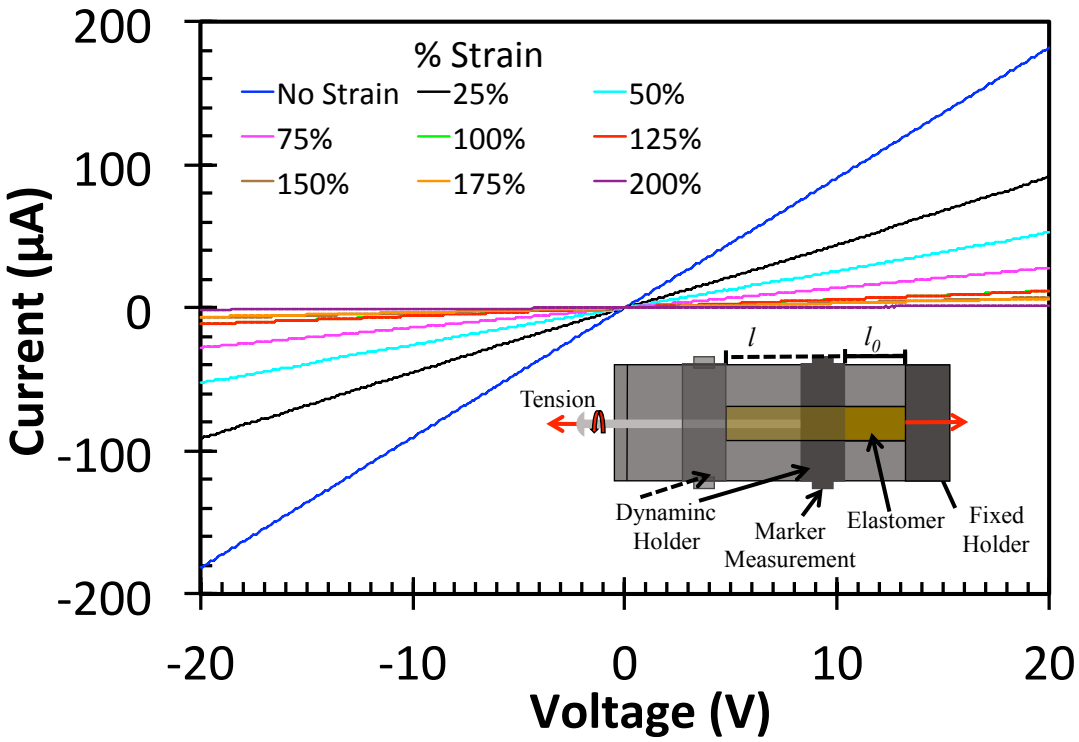

Figure 4.30 I-V response of elastomer (rubber band) treated in NMP:water:graphite/graphene solution with 37.5 mg mL^{-1} of graphite/graphene concentration at strains. Schematic of rubber band tensile mechanism is also shown.

For both concentrations, the most current sensitive region happened to be up to 50% strain, shown in Figure 4.31, in which the sensitivity rate are for concentration 37.5 mg mL-^{1} was 0.90 V μA at

7 V, 0.65 V µA at 5 V, and 0.39 V µA at 3 V and for concentration 75 mg mL^{-1} was 0.90 V µA at 7 V, 0.64 V µA at 5 V, and 0.38 V µA at 3 V, which means that in terms of sensitivity up to 50 % strain both composites can be used for similar strain sensors.

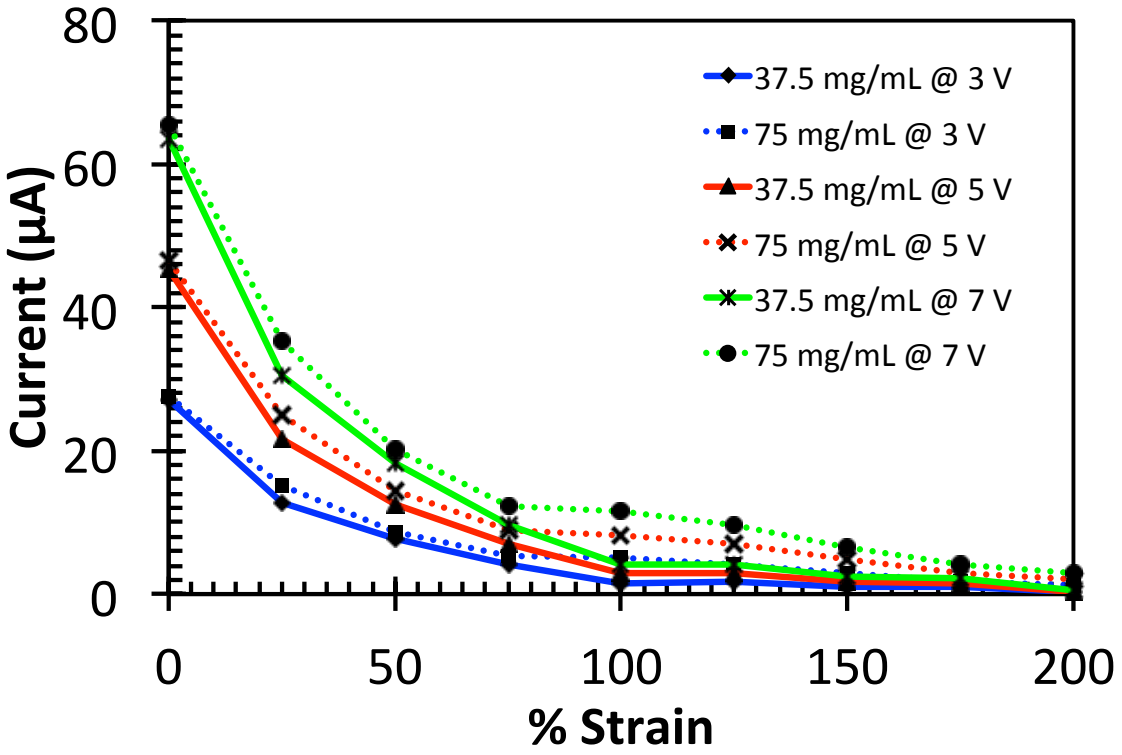

Figure 4.31 Current v. % strain at 3, 5 and 7 V for composites of treated rubber bands at 37.5 and 75 mg mL^{-1} of graphite/graphene dispersed in NMP:water solution.

CHAPTER 5: CONCLUSION

Two-dimensional (2D) layered materials, specifically MoS_2, WS_2, and graphite, were studied here using solution dispersion techniques along with a non-layered material, Aluminum powder. All four of these materials were subject to chemical liquid exfoliation under ultra-sonication in NMP solvent at a constant power of the sonicator and concentration. Once these materials were exposed to these experimental conditions, the layer number of the exfoliated MoS_2 and graphite using Raman spectroscopy revealed the presence of few layer nanoplatelets. Similarly, the particle size distribution analysis, as appeared to be a promising characterization technique to evaluate treated materials, from which it was concluded that the greatest effect or change in particle size occurred during the initial 30 minutes under ultra-sonication for the 2D layered materials, in contrast to Al which showed a fragmentation rate of zero during the initial 30 minutes of sonication time. Other characterization techniques were also utilized, specifically Scanning Electron Microscopy (SEM) and X-Ray Diffraction (XRD) analysis, from which the structural effects of the sonication on the materials investigated were unveiled. In particular, a shift in the characteristic peaks of the XRD spectra as a function of the sonication time was correlated to the induced stresses on the crystal structure in all of the materials investigated.

Such treated samples were introduced into polymer matrices, specifically an elastomer and an acrylic, to evaluate the optical and electrical properties of these composite structures. MoS_2, WS_2, and Aluminum did not produce electrical signals because of the high resistance present in the composite. On the other hand, graphite:polymer composites provided optical and electrical data; in each case, different behaviors were discovered. In the case of the rubber band or elastomer composite, I-V response showed ohmic behavior because of the linear reaction. For graphite:acrylic composite ohmic and non-ohmic behavior were observed. It was suggested that, in the case of the acrylic composites, percolation theory

and tunneling effect alongside compressive and tensile modes serve as a route to understand each observed behavior.

Through this thesis work, powder materials were successfully exposed to chemical liquid exfoliation. Moreover, hybrid materials were formulated, which provided attractive optical and electrical properties during elastic deformation and as a function of strain. The material composites that were created throughout this work serve as baseline for future work in opto-electro-mechanical devices.

REFERENCES

Albrecht, T. R., H. A. Mizes, J. Nogami, Sang Il Park, and C. F. Quate. 1988. "Observation of Tilt Boundaries in Graphite by Scanning Tunneling Microscopy and Associated Multiple Tip Effects." *Applied Physics Letters* 52 (5): 362–64. doi:10.1063/1.99465.

Amjadi, Morteza, Aekachan Pichitpajongkit, Sangjun Lee, Seunghwa Ryu, and Inkyu Park. 2014. "Highly Stretchable and Sensitive Strain Sensor Based on Silver Nanowire-Elastomer Nanocomposite." *ACS Nano* 8 (5): 5154–63. doi:10.1021/nn501204t.

Bagri, Akbar, Sang Pil Kim, Rodney S. Ruoff, and Vivek B. Shenoy. 2011. "Thermal Transport across Twin Grain Boundaries in Polycrystalline Graphene from Nonequilibrium Molecular Dynamics Simulations." *Nano Letters* 11 (9): 3917–21. doi:10.1021/nl202118d.

Balberg, I., D. Azulay, D. Toker, and O. Millo. 2004. "Percolation and Tunneling in Composite Materials." *International Journal of Modern Physics B* 18 (15): 2091–2121. doi:10.1142/S0217979204025336.

Boland, Conor S., Umar Khan, Claudia Backes, Arlene O'Neill, Joe McCauley, Shane Duane, Ravi Shanker, et al. 2014. "Sensitive, High-Strain, High-Rate Bodily Motion Sensors Based on Graphene-Rubber Composites." *ACS Nano* 8 (9): 8819–30. doi:10.1021/nn503454h.

Carey, Benjamin J, Torben Daeneke, Emily P Nguyen, and Yichao Wang. 2015. "Two Solvent Grinding Sonication Method for the Synthesis of Two-Dimensional Tungsten Disulphide Flakes †." *Chemical Communications* 51. Royal Society of Chemistry: 3770–73. doi:10.1039/C4CC08399G.

Castro Neto, A. H.., N. M. R.. Peres, K. S.. Novoselov, A. K.. Geim, and F. Guinea. 2009. "The Electronic Properties of Graphene." *Reviews of Modern Physics* 81 (1): 109–62. doi:10.1103/RevModPhys.81.109.

Červenka, J., and C. F J Flipse. 2009. "Structural and Electronic Properties of Grain Boundaries in Graphite: Planes of Periodically Distributed Point Defects." *Physical Review B - Condensed Matter and Materials Physics* 79 (19). doi:10.1103/PhysRevB.79.195429.

Clemmer, C R, and T P Beebe. 1991. "Graphite: A Mimic for DNA and Other Biomolecules in Scanning Tunneling Microscope Studies." *Science (New York, N.Y.)* 251 (4994): 640–42. doi:10.1126/science.1992517.

Coleman, J. N., M. Lotya, A. O'Neill, S. D. Bergin, P. J. King, U. Khan, K. Young, et al. 2011. "Two-Dimensional Nanosheets Produced by Liquid Exfoliation of Layered Materials." *Science* 331 (6017): 568–71. doi:10.1126/science.1194975.

Coleman, Jonathan N. 2013. "Liquid Exfoliation of Defect-Free Graphene." *Accounts of Chemical Research* 46 (1): 14–22. doi:10.1021/ar300009f.

Cunningham, Graeme, Mustafa Lotya, Clotilde S. Cucinotta, Stefano Sanvito, Shane D. Bergin, Robert Menzel, Milo S P Shaffer, and Jonathan N. Coleman. 2012. "Solvent Exfoliation of Transition Metal Dichalcogenides: Dispersibility of Exfoliated Nanosheets Varies Only Weakly between Compounds." *ACS Nano* 6 (4): 3468–80. doi:10.1021/nn300503e.

Delgado, Alberto Jorge A. Catalan, Hisato Yamaguchi, Claudia Narvaez Villarrubia, Aditya D. Mohite, and Anupama B. Kaul. 2016 "Characterization of 2D MoS_2 and WS_2 Dispersed in Organic Solvents for Composite Applications." Spring MRS Meeting. Phoenix, AZ.

Delgado, Alberto Jorge A. Catalan, Hisato Yamaguchi, Claudia Narvaez Villarrubia, Aditya D. Mohite, and Anupama B. Kaul. 2016 "Solvent Dispersed Two-dimensional Layered Materials: Characterization and Application in Opto-electro-mechanical Percolative Composites." Summited to Advanced Materials Journal (in review).

Geim, A K. 2009. "Graphene: Status and Prospects." *Science (New York, N.Y.)* 324 (5934): 1530–34. doi:10.1126/science.1158877.

Geim, A K, and K.S. Novoselov. 2007. "The Rise of Graphene." *Nature Mater.* 6 (3): 183–91. doi:10.1038/nmat1849.

Giorgino, Toni, Paolo Tormene, Federico Lorussi, Danilo De Rossi, and Silvana Quaglini. 2009. "Sensor Evaluation for Wearable Strain Gauges in Neurological Rehabilitation." *IEEE Transactions on Neural Systems and Rehabilitation Engineering* 17 (4): 409–15. doi:10.1109/TNSRE.2009.2019584.

Grantab, Rassin, Vivek B Shenoy, and Rodney S Ruoff. 2010. "Anomalous Strength Characteristics of Tilt Grain Boundaries in Graphene." *Science (New York, N.Y.)* 330 (6006): 946–48. doi:10.1126/science.1196893.

Hempel, Marek, Daniel Nezich, Jing Kong, and Mario Hofmann. 2012. "A Novel Class of Strain Gauges Based on Layered Percolative Films of 2D Materials." *Nano Letters* 12 (11): 5714–18. doi:10.1021/nl302959a.

Hernandez, Yenny, Valeria Nicolosi, Mustafa Lotya, Fiona M Blighe, Zhenyu Sun,

Sukanta De, I T McGovern, et al. 2008. “High-Yield Production of Graphene by Liquid-Phase Exfoliation of Graphite.” *Nature Nanotechnology* 3 (9): 563–68. doi:10.1038/nnano.2008.215.

Hill, Ernie W., Aravind Vijayaragahvan, and Kostya Novoselov. 2011. “Graphene Sensors.” *IEEE Sensors Journal* 11 (12): 3161–70. doi:10.1109/JSEN.2011.2167608.

Hu, Y., X. Li, a. Lushington, M. Cai, D. Geng, M. N. Banis, R. Li, and X. Sun. 2013. “Fabrication of MoS_2-Graphene Nanocomposites by Layer-by-Layer Manipulation for High-Performance Lithium Ion Battery Anodes.” *ECS Journal of Solid State Science and Technology* 2 (10): M3034–39. doi:10.1149/2.007310jss.

Huang, Mingyuan, Hugen Yan, Tony F. Heinz, and James Hone. 2010. “Probing Strain-Induced Electronic Structure Change in Graphene by Raman Spectroscopy.” *Nano Letters* 10 (10): 4074–79. doi:10.1021/nl102123c.

Jariwala, Deep, Vinod K. Sangwan, Lincoln J. Lauhon, Tobin J. Marks, and Mark C. Hersam. 2014. “Emerging Device Applications for Semiconducting Two-Dimensional Transition Metal Dichalcogenides.” *ACS Nano* 8 (2): 1102–20. doi:10.1021/nn500064s.

Jawaid, Ali, Dhriti Nepal, Kyoungweon Park, Michael Jespersen, Anthony Qualley, Peter Mirau, Lawrence F. Drummy, and Richard A. Vaia. 2015. “Mechanism for Liquid Phase Exfoliation of MoS_2.” *Chemistry of Materials*, acs.chemmater.5b04224. doi:10.1021/acs.chemmater.5b04224.

Kaltenbrunner, Martin, Tsuyoshi Sekitani, Jonathan Reeder, Tomoyuki Yokota, Kazunori Kuribara, Takeyoshi Tokuhara, Michael Drack, et al. 2013. “An Ultra-Lightweight Design for Imperceptible Plastic Electronics.” *Nature* 499 (7459): 458–63. doi:10.1038/nature12314.

Katsnelson, Mikhail I. 2007. “Graphene: Carbon in Two Dimensions.” *Materials Today*. doi:10.1016/S1369-7021(06)71788-6.

Khan, Umar, Arlene O’Neill, Mustafa Lotya, Sukanta De, and Jonathan N. Coleman. 2010. “High-Concentration Solvent Exfoliation of Graphene.” *Small* 6 (7): 864–71. doi:10.1002/smll.200902066.

Lahiri, Jayeeta, You Lin, Pinar Bozkurt, Ivan I Oleynik, and Matthias Batzill. 2010. “An Extended Defect in Graphene as a Metallic Wire.” *Nature Nanotechnology* 5 (5): 326–29. doi:10.1038/nnano.2010.53.

Liu, Chao Xuan, and Jin W. Choi. 2009. “An Embedded PDMS Nanocomposite Strain Sensor toward Biomedical Applications.” In *Proceedings of the 31st Annual*

International Conference of the IEEE Engineering in Medicine and Biology Society: Engineering the Future of Biomedicine, EMBC 2009, 6391–94. doi:10.1109/IEMBS.2009.5333873.

Liu, Chao-Xuan, and Jin-Woo Choi. 2009. "Patterning Conductive PDMS Nanocomposite in an Elastomer Using Microcontact Printing." *Journal of Micromechanics and Microengineering* 19 (8): 085019. doi:10.1088/0960-1317/19/8/085019.

Liu, Yuanyue, and Boris I. Yakobson. 2010. "Cones, Pringles, and Grain Boundary Landscapes in Graphene Topology." *Nano Letters* 10 (6): 2178–83. doi:10.1021/nl100988r.

Lorussi, Federico, Enzo Pasquale Scilingo, Mario Tesconi, Alessandro Tognetti, and Danilo De Rossi. 2005. "Strain Sensing Fabric for Hand Posture and Gesture Monitoring." *IEEE Transactions on Information Technology in Biomedicine* 9 (3): 372–81. doi:10.1109/TITB.2005.854510.

Malola, Sami, Hannu Häkkinen, and Pekka Koskinen. 2010. "Structural, Chemical, and Dynamical Trends in Graphene Grain Boundaries." *Physical Review B - Condensed Matter and Materials Physics* 81 (16). doi:10.1103/PhysRevB.81.165447.

Mesaros, A., S. Papanikolaou, C. F. J. Flipse, D. Sadri, and J. Zaanen. 2010. "Electronic States of Graphene Grain Boundaries." *Physical Review B* 82 (20): 205119. doi:10.1103/PhysRevB.82.205119.

Michel, Monica, Dalal Fadil, Gustavo A. Lara, Alberto Delgado, Christopher Gaytan,Esteban Escarcega, and Anupama Kaul. 2015. "Material characterization of 2D layered crystals for printed electronics applications." Poster Presentation NSF US – EU Workshop on 2D Layered Materials & Devices. Arlington, VA.

Michel, Monica, Dalal Fadil, Alberto Delgado, Gustavo A. Lara, Esteban Escaraga and Anupama B. Kaul. 2015. " Material Characterization of Van der Waals Solids for Solution Based Applications". Poster Presentation IEEE Photonics Society Conference. Nassau, Bahamas

Michel, Monica, Jay Desai, Alberto Delgado and Anupama B. Kaul. 2016. "Optimization of fluid characteristics of 2D materials for inkjet." Poster Presentation Spring MRS Meeting. Phoenix, AZ.

Novoselov, K S, V I Fal'ko, L Colombo, P R Gellert, M G Schwab, and K Kim. 2012. "A Roadmap for Graphene." *Nature* 490 (7419): 192–200. doi:10.1038/nature11458.

Ovchinnikov, Dmitry, Adrien Allain, Ying Sheng Huang, Dumitru Dumcenco, and

Andras Kis. 2014. “Electrical Transport Properties of Single-Layer WS_2.” *ACS Nano* 8 (8): 8174–81. doi:10.1021/nn502362b.

Pantelopoulos, Alexandros, and Nikolaos G. Bourbakis. 2010. “A Survey on Wearable Sensor-Based Systems for Health Monitoring and Prognosis.” *IEEE Transactions on Systems, Man and Cybernetics Part C: Applications and Reviews*. doi:10.1109/TSMCC.2009.2032660.

Paton, Keith R., Eswaraiah Varrla, Claudia Backes, Ronan J. Smith, Umar Khan, Arlene O’Neill, Conor Boland, et al. 2014. “Scalable Production of Large Quantities of Defect-Free Few-Layer Graphene by Shear Exfoliation in Liquids.” *Nature Materials* 13 (6): 624–30. doi:10.1038/nmat3944.

Pereira, Vitor M., and A. H. Castro Neto. 2009. “Strain Engineering of Graphene’s Electronic Structure.” *Physical Review Letters* 103 (4). doi:10.1103/PhysRevLett.103.046801.

Peres, N. M R, F. Guinea, and A. H. Castro Neto. 2006. “Electronic Properties of Disordered Two-Dimensional Carbon.” *Physical Review B - Condensed Matter and Materials Physics* 73 (12). doi:10.1103/PhysRevB.73.125411.

Rautaray, S S, and A Agrawal. 2011. *Interaction with Virtual Game through Hand Gesture Recognition*. *2011 International Conference on Multimedia, Signal Processing and Communication Technologies*. doi:10.1109/mspct.2011.6150485.

Rogers, John A, Takao Someya, and Yonggang Huang. 2010. “Materials and Mechanics for Stretchable Electronics.” *Science (New York, N.Y.)* 327 (2010): 1603–7. doi:10.1126/science.1182383.

Rosenberger, M, G Koller, S Belle, B Schmauss, and R Hellmann. 2012. “Planar Bragg Grating in Bulk Polymethylmethacrylate.” *Optics Express* 20 (25): 27288–96. doi:10.1364/OE.20.027288.

Tao, L, H Long, B Zhou, S F Yu, S P Lau, Y Chai, K H Fung, Y H Tsang, J Yao, and D Xu. 2014. “Preparation and Characterization of Few-Layer MoS_2 Nanosheets and Their Good Nonlinear Optical Responses in the PMMA Matrix.” *Nanoscale* 6 (16). Royal Society of Chemistry: 9713–19. doi:10.1039/c4nr02664k.

Yamada, Takeo, Yuhei Hayamizu, Yuki Yamamoto, Yoshiki Yomogida, Ali Izadi-Najafabadi, Don N Futaba, and Kenji Hata. 2011. “A Stretchable Carbon Nanotube Strain Sensor for Human-Motion Detection.” *Nature Nanotechnology* 6 (5): 296–301. doi:10.1038/nnano.2011.36.

Yao, Shanshan, and Yong Zhu. 2014. “Wearable Multifunctional Sensors Using Printed

Stretchable Conductors Made of Silver Nanowires." *Nanoscale* 6 (4): 2345. doi:10.1039/c3nr05496a.

Yazyev, Oleg V., and Steven G. Louie. 2010a. "Topological Defects in Graphene: Dislocations and Grain Boundaries." *Physical Review B - Condensed Matter and Materials Physics* 81 (19). doi:10.1103/PhysRevB.81.195420.

Yazyev, Oleg V, and Steven G Louie. 2010b. "Electronic Transport in Polycrystalline Graphene." *Nature Materials* 9 (10): 806–9. doi:10.1038/nmat2830.

Yu, Yan, Shenglin Jiang, Wenli Zhou, Xiangshui Miao, Yike Zeng, Guangzu Zhang, and Sisi Liu. 2013. "Room Temperature Rubbing for Few-Layer Two-Dimensional Thin Flakes Directly on Flexible Polymer Substrates." *Scientific Reports* 3 (2): 2697. doi:10.1038/srep02697.

VITA

Alberto Delgado was born in El Paso, Texas. The second oldest son of Armando Delgado and Maria De La Paz Ivione Marentes Cardona, he graduated from J. M. Hanks High School in spring 2009 and joined the Mechanical Engineering program at The University of Texas at El Paso in the Fall of 2009. While pursuing a Bachelor's degree in Mechanical Engineering, he worked at the Mechanical Engineering Machine Shop, in which he developed a passion to metals and materials and decided to also join the Metallurgical and Materials Engineering program. Besides working in the Machine Shop as an undergraduate student, he conducted research on ultra-high temperature materials during the Fall of 2012 under Professor Arturo Bronson, Ph.D. the supervisor for a Department of Energy sponsored project. During the Spring of 2013 he was appointed for a semester and summer-long internship to work at Halliburton Energy and Services Co. under the Materials group in the Technology Department at Houston, TX. Upon graduation, he agreed and participated once more in a summer-long internship in 2014 at Halliburton Energy and Services Co. Once he earned his double major, he decided to continue his education and enroll into Graduate School at The University of Texas at El Paso for fall of 2014. As a graduate student, he worked as a Research Assistant, and together with Professor Anupama Kaul, Ph.D., performed research for an Army Research Office sponsored project.

Permanent address: 11574 Bob Mitchell Dr.
El Paso, TX 79936

This thesis was typed by Alberto Delgado.